



Escola d'Enginyeria de Telecomunicació i
Aeroespacial de Castelldefels

UNIVERSITAT POLITÈCNICA DE CATALUNYA

TREBALL FINAL DE GRAU

TFG TITLE: Numerical simulation of fluids in microfluidics (microgravity conditions) with OpenFOAM

DEGREE: Grau en Enginyeria d'Aeroports

AUTHOR: Nuria López García

ADVISOR: Santiago Arias Calderón

DATE: 19th January 2023

Título: Numerical simulation of fluids in microfluidics (microgravity conditions) with OpenFOAM

Autor: Nuria López García

Director: Santiago Arias Calderón

Fecha: 19 de enero del 2023

Resumen

Durante las últimas décadas, el interés por los microfluidos basados en la generación de gotas ha aumentado sustancialmente debido a su amplia gama de aplicaciones, como en la bioquímica o en la síntesis de materiales. Por tanto, es fundamental predecir y comprender el mecanismo de generación de estas gotas para poder controlar su tamaño y, posteriormente, diseñar los dispositivos necesarios para producirlas.

Este trabajo presenta simulaciones numéricas de dos líquidos en un microcanal rectangular con forma de T con un estrechamiento, bajo condiciones de microgravedad. El estudio se ha realizado siguiendo las mismas características que el artículo científico [1], con el propósito de hacer una comparación fidedigna entre los dos y poder verificar los resultados obtenidos. Por tanto, los líquidos utilizados serán agua desionizada para la fase dispersa y aceite de girasol para la continua.

El *software* utilizado para realizar estas simulaciones numéricas ha sido OpenFOAM y el *solver* escogido ha sido *InterFoam*, que es ideal para dos fluidos incompresibles, isoterms e inmiscibles considerando que utiliza el método *Volume Of Fluid* (VOF). Para procesar los datos obtenidos, también se han empleado los programas de ParaView y Excel.

Muchos parámetros se han tenido en cuenta y se han modificado a lo largo de las simulaciones hasta encontrar el ajuste más apropiado, como las condiciones de contorno, la calidad de la malla o la longitud del microcanal. Las principales variables seleccionadas para analizar han sido el diámetro y el volumen de las gotas generadas.

Finalmente, el estudio concluye que los resultados obtenidos durante las simulaciones no son del todo parecidos al artículo que se pretende reproducir, obteniendo unos errores significativos en el volumen de las gotas. Además, el número de burbujas generadas es mayor al esperado, haciendo que sea difícil determinar si este experimento en concreto se puede replicar satisfactoriamente usando el método de Dinámica de Fluidos Computacional (CFD).

Title: Numerical simulation of fluids in microfluidics (microgravity conditions) with OpenFOAM

Author: Nuria López García

Director: Santiago Arias Calderón

Date: 19th January 2023

Overview

During the past decades, interest in droplet-based microfluidics has substantially increased due to its wide range of applications, such as biochemical analyses or material synthesis. Therefore, it is essential to predict and understand these droplets' generation mechanisms to control their size and, eventually, design the precise devices to produce them.

This work presents numerical simulations of two phases of liquids in a rectangular T-shaped microchannel with a neck under microgravity conditions. The study will be made following the same scenario as the scientific paper [1], to do a trustworthy comparison between the two of them and verify the obtained results. Consequently, the liquids used will be deionized water for the dispersed phase and sunflower oil for the continuous one.

The software utilised to carry out these numerical simulations was OpenFOAM. The chosen solver was InterFOAM, which is ideal for two incompressible, isothermal and immiscible fluids; considering that it uses the Volume Of Fluid (VOF) method. To process the obtained data, ParaView and Excel were used as well.

Many parameters were modified and taken into account when performing the simulations until the perfect fit was found, such as the boundary conditions, the mesh quality or the microchannel length. After that, the main selected variables to analyse were the diameter, the volume and the velocity of the generated droplets.

Finally, the study concludes that the results obtained during the simulations are not in good agreement with the literature, obtaining significant errors in the droplets volume. Moreover, the produced number of droplets is bigger than the expected. Taking all this into account, it is not possible to say that the Computational Fluid Dynamics (CFD) method is an accurate one when we aim to perform this type of experiment.

INDEX

ACKNOWLEDGEMENTS	1
CHAPTER 1. INTRODUCTION.....	3
1.1 Microgravity	3
1.1.1 Orbiting microgravity facilities	4
1.1.2 Non-orbiting microgravity facilities	4
1.1.3 Ground microgravity simulators	5
1.1.4 Ground microgravity analogues.....	7
1.2. Microfluidics	8
1.2.1. Droplet-based microfluidics	9
1.3. Aim of the project.....	10
CHAPTER 2. PROBLEM STATEMENT AND METHODOLOGY	12
2.1 Review of the article.....	12
2.2. Problem statement	15
2.2.1 Fluid characteristics	15
2.2.2 Context verification	17
2.2.3 Contact angle	19
2.3 Methodology: CFD	20
2.3.1 Pre-processing	21
2.3.2 Solver	23
2.3.3 Post-processing.....	25
CHAPTER 3. EVOLUTION OF THE SIMULATIONS	27
3.1 Early stages	27
3.2 Fundamental probing.....	32
3.2.1 Mesh definition	32
3.2.2 Boundary conditions evaluation.....	35
3.2.3 Validation of the solution.....	39
3.3 Final data gathering	40
CHAPTER 4. RESULTS	45
4.1 Analysis of the droplet diameter.....	46
4.2 Analysis of the droplet volume	49
CHAPTER 5. CONCLUSIONS.....	53

BIBLIOGRAPHY	55
APPENDIX A. OPENFOAM.....	59
A.1 Case folder.....	59
A.1.1 0 folder.....	59
A.1.2 Constant folder	65
A.1.3 System folder.....	67
A.2 How to run a simulation.....	72
A.3 ParaView	73
APPENDIX B. RESULTS.....	76
APPENDIX C. BOUNDARY CONDITIONS	79
C.1 Outlet boundary conditions.....	79
C.2 Contact angles.....	80
C.2.1 Boundary conditions evaluation.....	80
C.2.2 Results.....	83

LIST OF FIGURES

Fig. 1.1 Schematic representation of (a) drop tower; (b) parabolic flight; and (c) sounding rocket [7].....	5
Fig. 1.2 Altitude in km of orbiting (CubeSat, ISS) and non-orbiting (sounding rockets, parabolic flights) facilities and atmospheric zones [7].....	5
Fig. 1.3 Schematic representation of (a) 1D clinostat; (b) 2D clinostat; (c) 3D clinostat/RPM; and (d) diamagnetic levitation system [7].....	6
Fig. 1.4 Schematic representation of bed rest (top) and dry immersion (bottom)7	
Fig. 1.5 Example of microfluidics application for a spiral microfluidic chip [11]... 8	
Fig. 1.6 Diverse structures for droplet generation. (A) Cross-flowing structure, (B) Flow-focusing structure and (C) Co-flowing structure [12].....	9
Fig. 1.7 Sketch of the T-junction case	10
Fig. 2.1 Paper's graphic showing the three different stages for a droplet generation period [1]	13
Fig. 2.2 Effects of the flow rate on droplet diameter depending on the Ca_c (a) and α (b) [1].....	13
Fig. 2.3 Normalized droplet volumes of experiments and their fitted curves varied with the Ca_c under uniform flow rate ratio α (a); α under uniform Ca_c (b).....	14
Fig 2.4 Description of the contact angle [24]	20
Fig. 2.5 CFD analysis of velocity field around an airfoil [27].....	21
Fig. 2.6 Geometry used in the scientific paper [1]	22
Fig. 2.7 Geometry with its boundaries	22
Fig. 2.8 Overview of the OpenFOAM software directory structure used.....	24
Fig. 2.9 Dynamics of droplet formation and droplet size in the T-junction with a neck [1].....	26
Fig. 2.10 Example of a simulation with $Q_c = Q_d = 6\mu l/min$	26
Fig. 3.1 Basic geometry for the simulations and dimensions.....	27
Fig. 3.2 First geometry for the initial simulations and dimensions.	28
Fig. 3.3 First mesh for the first geometry	29
Fig. 3.4 Experimental droplet generation period with its time steps [1].....	31
Fig. 3.5 Evolution of the droplet formation in the simulation for the boundary conditions chosen	31
Fig. 3.6 Second geometry for the simulations with its dimensions	33
Fig. 3.7 First mesh for the second geometry	33
Fig. 3.8 Comparison simulation between the first and the second geometry with the same mesh.....	34

Fig. 3.9 The second mesh used for the new geometry.....	34
Fig. 3.10 Comparison simulation between the less dense mesh and a denser one.....	35
Fig. 3.11 Example of suction of the droplets at the outlet.....	36
Fig. 3.12 Droplet diameter at the outlet	37
Fig. 3.13 Comparison between the mesh with half the cells (A) and the one with the double (B).....	38
Fig. 3.14 Evolution of the droplet formation for the boundary conditions chosen.	39
Fig. 3.15 New mesh for the complete geometry	40
Fig. 3.16 The three meshes used; the top one (n/2), the middle one (n) and the bottom one (nx2)	41
Fig. 3.17 Close-up look at walls1 and 2 at 0°, 15° and 30°, respectively	43
Fig. 4.1 Comparison between experimental and simulated data of the dependence of droplet diameter on Ca_c under the same α	47
Fig. 4.2 Comparison between experimental and simulated data of the dependence of droplet diameter on α under the same Ca_c	48
Fig. 4.3 Comparison between experimental and simulated data of the dependence of the normalized droplet volume on Ca_c under the same α .	50
Fig. 4.4 Comparison between experimental and simulated data of the dependence of the normalized droplet volume on α under the same Ca_c .	51
Fig. A.1 <i>alpha.oil</i> file	61
Fig. A.2 <i>p_rgh</i> file	63
Fig. A.3 <i>U</i> file.....	65
Fig. A.4 <i>transportProperties</i> file	66
Fig. A.5 <i>turbulenceProperties</i> file	66
Fig. A.6 <i>g</i> file	67
Fig. A.7 <i>controlDict</i> file	68
Fig. A.8 <i>decomposeParDict</i> file	69
Fig. A.9 <i>fvSchemes</i> file.....	70
Fig. A.10 <i>fvSolution</i> file.....	71
Fig. A.11 <i>setFieldsDict</i> file.....	71
Fig. A.12 General view of the ParaView window	73
Fig. A.13 Close-up of the top part tools	74
Fig. A.14 ParaView window with the <i>slice</i> tool.....	74
Fig. A.15 ParaView window with the <i>ruler</i> tool.....	75
Fig. B.1 Scheme of the droplet for the measures	76
Fig. B.2 First part of the results table.....	77

Fig. B.3 Second part of the results table	78
Fig. C.1 Boundary conditions trial.....	79
Fig. C.2 First part of the contact angle trial.....	80
Fig. C.3 Second part of the boundary conditions trial	81
Fig. C.4 Plot of the different normalized volume for every simulation	82
Fig. C.5 Plot of the different diameters for the following simulations	82
Fig. C.6 Contact angles for the final simulations	83

LIST OF TABLES

Table 2.1 Fluid properties values	16
Table 2.2 Maximum and minimum dimensionless numbers values.....	19
Table 2.3 Dimensions of the T-shape channel with a neck	22
Table 2.4 Simulation time depending on the number of cores.....	25
Table 3.1 Review of the boundary conditions in the alpha file.....	29
Table 3.2 Review of the boundary conditions in the pressure file.....	30
Table 3.3 Review of the boundary conditions in the velocity file.....	30
Table 3.4 Review of the interface dimension depending on the mesh	35
Table 3.5 Review of the droplet dimension depending on the mesh	38
Table 3.6 Summary of the different characteristics of each mesh	42
Table 4.1 Velocities and Capillary numbers for $\alpha = 1$	45
Table 4.2 Velocities and Capillary numbers for $\alpha = 0.5$	46
Table 4.4 Experimental vs. Simulation data for the diameter with the error	48
Table 4.5 Experimental vs. Simulation data for the volume with the error.	51

ACKNOWLEDGEMENTS

In the first place, I would really like to thank my advisor Santiago Arias Calderón for his guidance throughout this long and challenging project. He has provided me all the necessary tools, an uncountable number of meetings to track my progress and lead me to the next step, specially these last months when I was very close to finishing. He has been essential for the completion of this study. Thanks for your time and patience.

I would also like to thank my family, my partner and my friends for his unconditional support during these months, as well as, through the entire degree. They have always been there for me, they have believed in me and they have given me the love and comfort I needed at every step of the way. Without them it would have been impossible for me to achieve it and I am very grateful for having them.

CHAPTER 1. INTRODUCTION

During this initial part, a slight presentation of the main topics is going to be done, explaining what is microgravity and microfluidics. After that, the aim of the project will be expressed, just as the structure used.

1.1 Microgravity

It is well known that gravity is one of the main forces that drive the Earth since it drags objects towards its centre. It is measured as the attraction between any two objects with mass that are not in contact and at a certain distance, as stated Isaac Newton almost three and a half centuries ago [9]. The larger the masses of the objects, the stronger the pull between them and, for this reason, it weakens the further apart the objects are. Therefore, it is possible to say that microgravity is when the pull of gravity is very small or when the force of gravity is balanced with another force, making an object there seem weightless.

For example, when an object is orbiting around the Earth, gravity is constantly pulling it back towards the ground. However, this object is also moving so fast that it matches the Earth's curvature giving the sensation that it is falling around the Earth. This creates the sensation of weightlessness which are free-fall conditions and what is also known as microgravity [8].

Now we could be wondering, why do we seek these conditions if they seem so difficult to achieve. Well, the answer is quite simple, microgravity changes a lot of processes like crystal growth, fluid mixing, the separation between gases and liquids, heat transfer, solidification and combustion; for that reason, it is very important to study their behaviour. All this research could lead to the creation and development of new materials that cannot be made on Earth, due to gravity. These could have many new applications, such as, speeding up future computers, reducing pollution, improving fibre optics and enabling medical breakthroughs to cure diseases [5].

Over time, many agencies, such as NASA, have been studying and creating different methods and facilities in order to recreate these microgravity conditions and be able to do research experiments without needing to go out in space. However, they have been able to do it just for short periods of time, so the research still continues.

So far, there are four major ways in which these conditions can be achieved which are orbiting microgravity facilities (see subchapter 1.1.1), non-orbiting microgravity facilities (see subchapter 1.1.2), ground microgravity simulators (see subchapter 1.1.3) and ground microgravity analogues (see subchapter 1.1.4) [7].

1.1.1 Orbiting microgravity facilities

Long-term microgravity experiments can be performed on orbiting facilities which, includes space laboratories and autonomous microgravity laboratory platforms.

- International Space Station (ISS): is a modular space station in Low Earth Orbit which is in continuous free-fall. It is orbiting at 400 km high and at 28.000 km/h and it can serve as well as a microgravity research laboratory. It is the only platform where constant microgravity can be achieved, which is extremely useful when performing long term experiments.
- CubeSat: is a modular miniaturized satellite for space research. Each unit is a 10 x 10 cm cube with a mass of no more of 1.33 kg and each CubeSat can be constituted of up to 12 units. However, this method can only be applied in experiments that can be miniaturized. They usually orbit at an altitude between 350-700 km.

1.1.2 Non-orbiting microgravity facilities

Microgravity can be transiently achieved with non-orbiting microgravity facilities based on free-fall conditions, which are drop towers, parabolic flights and sounding rockets. These ones are widely used for short-term experiments.

- Drop towers: are very high towers from where you can drop your experiments, achieving weightlessness during the fall. In most cases, experiments are performed in an evacuated chamber to eliminate the effects of drag and friction forces. William Watts invented them in 1775 and one of the most important ones is ZARM, located in Bremen, Europe. This tower is 120 metres tall, however, a catapult was installed at the top of the building which doubles the free fall longitude by throwing the experiment upwards, obtaining 9.5 seconds of weightlessness.
- Parabolic flights: the aeroplane does a series of parabolas where they combine periods without lift and periods making up for the air's drag with its engines. When doing this, the only force we have inside the aircraft is gravity, so there is a free fall. Nevertheless, this method only reduces gravity to 10^{-2} and just 25 seconds of weightlessness are accomplished.
- Sounding rockets: are sub-orbital rockets that carry payloads above the atmosphere, without placing them into orbit around the Earth. Microgravity levels are around 10^{-5} and for 10 minutes approximately.

In Fig. 1.1 a representation of the non-orbiting microgravity facilities is shown. In (a) microgravity conditions are achieved in the middle of the fall from the tower, in (b) they are accomplished between the ups and downs of the aircraft's parabola and, finally in (c) they are reached when the payload is released and it falls.

In Fig. 1.2 it is possible to see the different altitudes at which orbiting and non-orbiting microgravity facilities work, as well as the atmospheric zones where it is possible to find them.

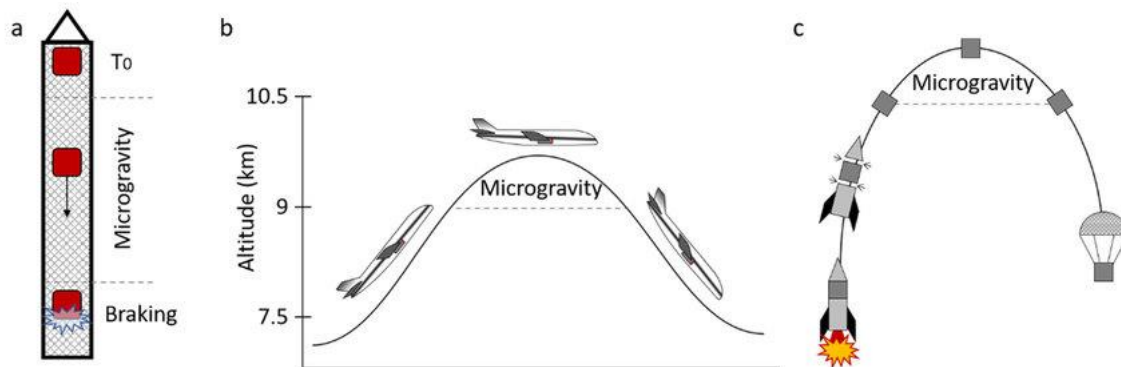


Fig. 1.1 Schematic representation of (a) drop tower; (b) parabolic flight; and (c) sounding rocket [7]

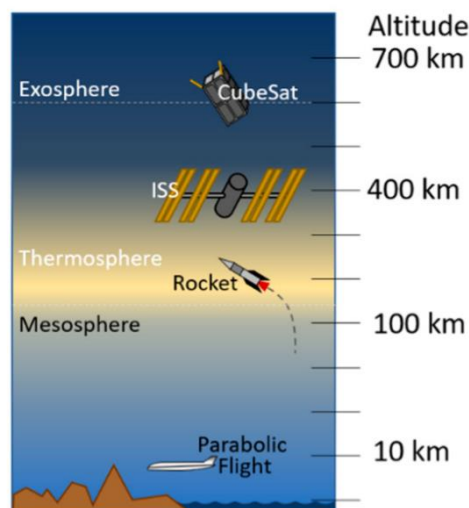


Fig. 1.2 Altitude in km of orbiting (CubeSat, ISS) and non-orbiting (sounding rockets, parabolic flights) facilities and atmospheric zones [7]

1.1.3 Ground microgravity simulators

Ground microgravity simulators do not reproduce microgravity conditions, they only reduce gravity using different methods, such as randomizing the direction of it over time or compensating the gravitational force with a counteracting force [7]. They are really useful tools for preparing spaceflight experiments and they also facilitate stand-alone studies, providing cost-efficient platforms for gravitational research. [6]

- Clinostat: they simulate the absence of a directional gravity input by averaging the gravity vector through rotation over time, even though they are unable to reproduce actual microgravity. They can rotate around one axis (1D or 2D clinostats) or around two axes (3D clinostats). Microgravity levels achieved vary between 10^{-3} (for 1D and 2D) and 10^{-4} (for 3D) and the duration for both of them vary between hours to weeks.
- Random positioning machine (RPM): they are like 3D clinostats but instead of spinning at constant speed and direction, they are randomized. These rotation induces accelerative forces, therefore in order to be able to use this method and obtain reliable data, the experimental conditions must be carefully set. Using this machine, the achieved microgravity is like in the 3D clinostat.
- Diamagnetic levitation: it compensates gravity at molecular level, by balancing the weight of water and biological tissues with the repulsive force exerted by a magnetic field. This method is very effective compensating gravity, however a strong magnetic field is created, influencing the sample. The microgravity created is around 10^{-2} with a varied duration from minutes to hours.

In Fig 1.3 the different ground microgravity simulators are shown. Clinostats (a) and (b) and RPM (c) simulate the absence of a directional gravity input by averaging the gravity vector through rotation around one or two axes over time. However, in (d), gravity is compensated at molecular level, by balancing the weight of water and biological tissues with the repulsive force exerted by a magnetic field. Within the magnetic field, a specimen can experience from zero (μg) to twice the gravity force (xg) depending on its position within the magnetic field gradient.

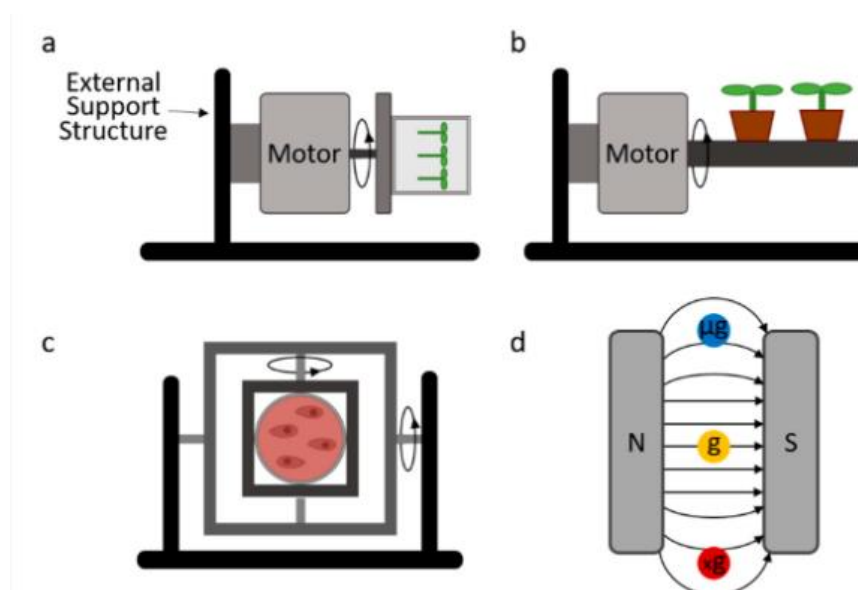


Fig. 1.3 Schematic representation of (a) 1D clinostat; (b) 2D clinostat; (c) 3D clinostat/RPM; and (d) diamagnetic levitation system [7]

1.1.4 Ground microgravity analogues

The effects of gravity can be reproduced using microgravity analogues, but only in physiological responses. Even though simulated microgravity conditions only reproduce some of the effects observed in a true microgravity environment, they represent effective, affordable, and readily available testbeds.

- Bed rest: it is used to simulate microgravity-associated inactivity in humans, in a normal gravitational environment. At first horizontal beds were used, but then they realised that 6° head-down tilt (HDT) was more effective because blood was redistributed from the legs to the head with its associated changes in physiological systems, mainly for bone, muscles and cardiovascular. However, it is not effective at compensating the effects of gravity on internal organs. The duration of bed rest experiments may vary from minutes to months.
- Dry immersion: It consists of head-out water immersion with subjects kept dry by the use of a waterproof, highly elastic fabric where, the buoyant force from air between the skin and the fabric lifts subjects under the water into a semi-recumbent posture. It accurately and rapidly reproduces most of the physiological effects of short-term spaceflight during days or even months.

In Fig. 1.4 a schematic of the two microgravity analogues is shown. In the top image the bed rest is represented, showing the 6° head-down tilt explained before, whereas in the bottom one, the dry immersion can be appreciated with the special posture and the waterproof fabric covering the body.

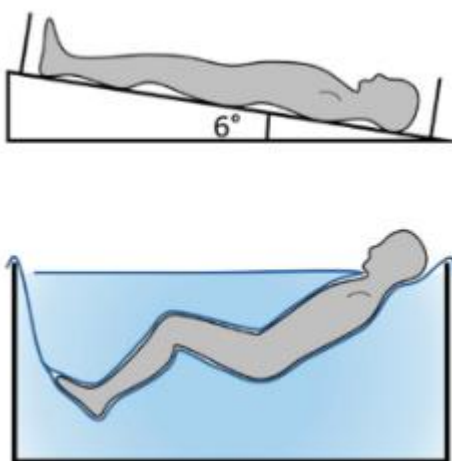


Fig. 1.4 Schematic representation of bed rest (top) and dry immersion (bottom)
[7]

1.2. Microfluidics

The term microfluidics refers to the study of the behaviour, accurate control and manipulation of fluids that are confined in micrometre scale. By decreasing the size of the experiment, it is possible to save storage space, time, money and materials, which is very useful when doing them in microgravity conditions.

On Earth, fluid handling often relies on gravity effects such as buoyancy and natural convection. In space, however, buoyancy effects are negligible due to the strong diminishment of gravity, resulting in the domination of surface tension forces. Surface tension forces are also dominating micro-scale processes in gravity, making microfluidics a promising technology for fluidic transport and handling in microgravity. The relevance of fluid handling in space is illustrated with everyday activities during space missions, such as drinking, plant watering, and gathering biometric data [10].

This science has many applications since it involves numerous fields, such as engineering, physics, chemistry, biochemistry, nanotechnology and biotechnology. Microfluidic systems are widely used in procedures such as DNA analysis, separation and manipulation of cells and cell patterning, including cancer and pathogen detection. Furthermore, they can be used to measure molecular diffusion coefficients, fluid viscosity and pH. Another interesting application is research, where antibiotic drug-resistant bacteria, nanoparticle transport in blood and observation of the chemical reaction kinetics are studied. It is well known that microfluidics has the potential to enable single-cell analysis which could allow significant investigations in molecular biology [12].

In Fig. 1.5 a spiral microfluidic chip can be seen. This device enables an ultrafast and efficient, size-based separation and isolation of circulating tumorous cells (CTCs), that appear at the early stages of cancer, from the whole blood.

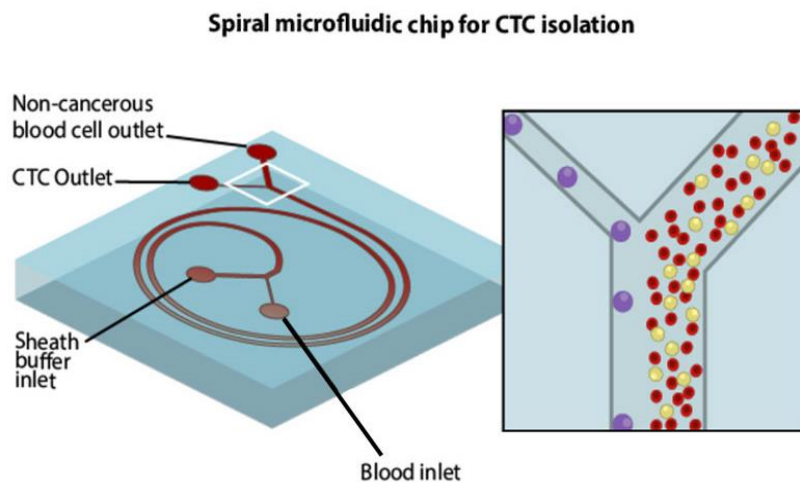


Fig. 1.5 Example of microfluidics application for a spiral microfluidic chip [11]

1.2.1. Droplet-based microfluidics

It is a subcategory of microfluidics, where the droplet generation is performed using passive or active methods. The active method involves the use of an external factor, such as an electric field, for the creation of the droplets. On the other hand, for the passive method, there is no external factor, it only depends on the geometry and the dimensions of the device [13]. Commonly, three types of geometries are used for passive droplet generation: cross-flowing, flow-focusing and co-flowing.

Droplets are formed because of the interaction between different immiscible flows, the dispersed and the continuous phase, which would be the droplets and the medium where they flow, respectively. Its sizes will depend, among other agents, on the velocity of each phase.

In Fig. 1.6 the three different geometries mentioned for the passive droplet generation can be seen, where the continuous phase is shown in blue and the dispersed phase in orange. In this study, the cross-flowing method will be the one used, so we will have the continuous and dispersed phases running at a certain angle to each other, in this case, in a T-junction.

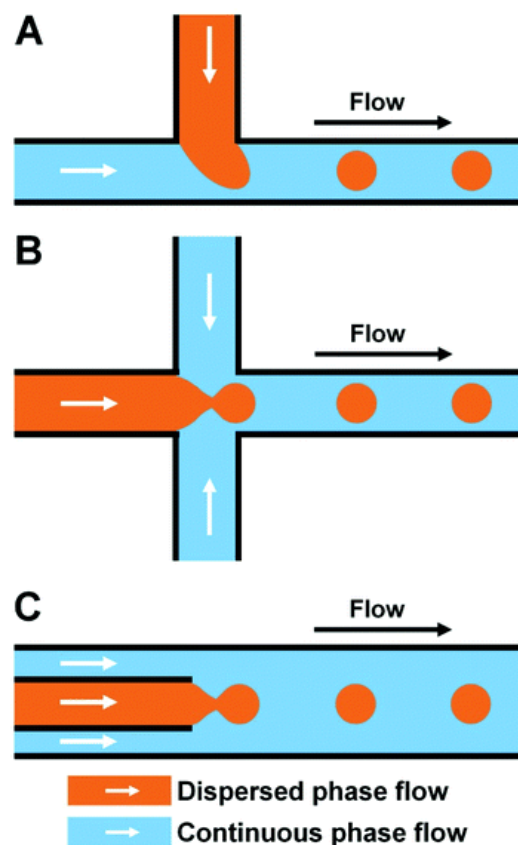


Fig. 1.6 Diverse structures for droplet generation. (A) Cross-flowing structure, (B) Flow-focusing structure and (C) Co-flowing structure [12]

1.3. Aim of the project

The main aim of this project is to recreate, as truthfully as possible, some of the experiments of the paper “Droplet generation under different flow rates in T-junction microchannel with a neck” [1] which will be summarized in Chapter 2, in order to prove that they can be performed using numerical simulations in OpenFOAM.

It is important to check if this kind of experiments can be recreated using simulations for different reasons. Proving the results are the same as in the real experiments, validates the use of these type of software, saving resources, time and money.

The experiment consists in a T-junction with a neck where oil is injected through the horizontal channel and water through the vertical one. With its interaction, droplets will be created, which will travel through the capillary until they leave through the outlet. In Fig. 1.7 a sketch of the case can be seen.

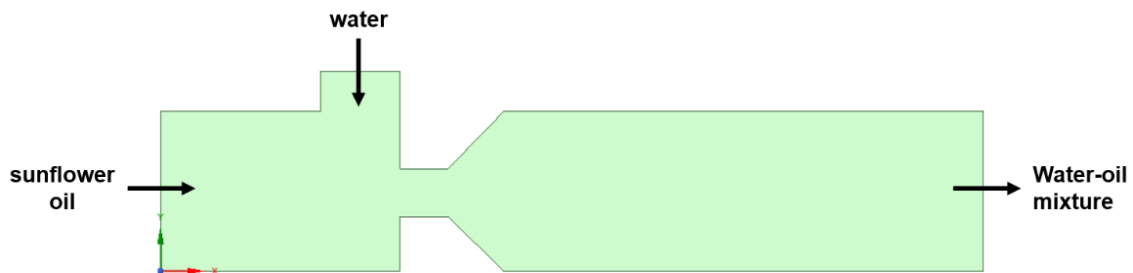


Fig. 1.7 Sketch of the T-junction case

For the purpose of doing this, the geometry and mesh will be created using a software named *Ansys* to, later on, introduce it in the main software which will be OpenFOAM to perform the numerical simulations.

After that, with the data collected, several plots will be done in order to study and analyse them to compare the results with the paper ones and see if the simulations have been successful or not.

After looking up at the article, some of the plots shown there were decided to be the ones that were going to be reproduced with the simulations. These plots showed different parameters such as the diameter and the volume of the droplets and will be seen in Chapter 2 when the summary of the paper will be done (see Fig. 2.2 and Fig 2.3).

Therefore, the organization for this project can be summarized as follows. In Chapter 2, the problem statement will be the introductory part to the review of the article, the fluids' characteristics, the diverse dimensionless numbers that take part in the study and the importance of the contact angle, as well as, exposing the different aids that were used in order to perform the simulations, which are mainly CFD and OpenFOAM. A deep description of the evolution of the experiments will be done in Chapter 3, explaining all the different geometries, meshes and variations between them during the three main stages of the project. In Chapter 4, the results will be presented and a discussion will be done for the parameters chosen, which are diameter and volume of the droplets. Eventually, the conclusions will be explained and a proposal for future work will be done in Chapter 5.

CHAPTER 2. PROBLEM STATEMENT AND METHODOLOGY

In this part of the project, a summary of the mentioned scientific paper will be done, as well as defining the experiment setting the fluid characteristics. Moreover, an explanation of the CFD science will be done, just like, its three different stages of the simulation process, which are the pre-processing, the simulation and the post-processing.

2.1 Review of the article

As was mentioned before, this project aims to make a comparison between the article's results and the ones obtained from the simulations by analysing some of the plots, specifically the ones that are shown here. Therefore, it is important to know a bit more about its content, this is why in this part of the study, a brief summary of it will be done.

The article "Droplet generation under different flow rates in T-junction microchannel with a neck" [1] written by a group of scientists from the Beijing University of Technology, targets to predict the size and volume of the droplets generated in a T-junction with a neck, but also, to prove that it can generate smaller droplets than in a normal T-junction.

A simple and widely used microfluidic channel to generate droplets is the T-junction, where two channels merge at a right angle, as well as, two immiscible liquids meet. The droplet size was proven to have a linear relationship with the flow rate ratio of the dispersed and the continuous phase, where the relation was initially reported to be independent of the fluid properties but affected by the dimension of geometries.

The shape of the formed droplets was observed and analysed, and it was determined that the droplet generation on both types of T-junctions, the normal and the one with a neck, was quite similar. Therefore, it could also be separated into three stages, including the filling stage, the squeezing stage and the breakup stage.

During the filling stage, the edge of the dispersed phase grows until it almost blocks the main channel. After that, the liquid moves along, the droplet starts growing and at the end of the squeezing stage, a neck starts to form due to the squeezing and shearing forces. Eventually, these forces make the droplet break at the neck and the cycle starts again with the beginning of the filling stage of another droplet (see Fig. 2.1).

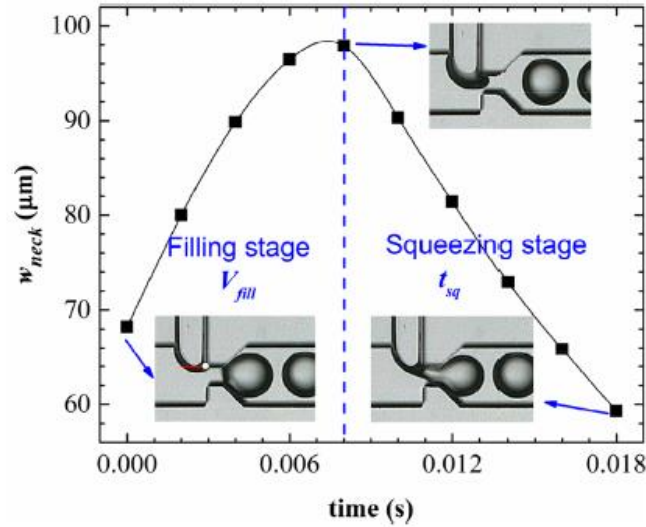


Fig. 2.1 Paper's graphic showing the three different stages for a droplet generation period [1]

The shape of the interface is formed by the force balance between the shear force, the surface tension force and the force of the upstream fluid pressure. The combination of these three forces leads to different shapes of the two liquids involved in this experiment and the generation of the stages mentioned before. The surface tension force is the one responsible for stabilizing the dispersed phase tip to hold back the breakup. Using the law of Newton's inner friction and the velocity vector, it was possible to provide the dynamics of liquids to, later on, obtain the shear force of the continuous phase.

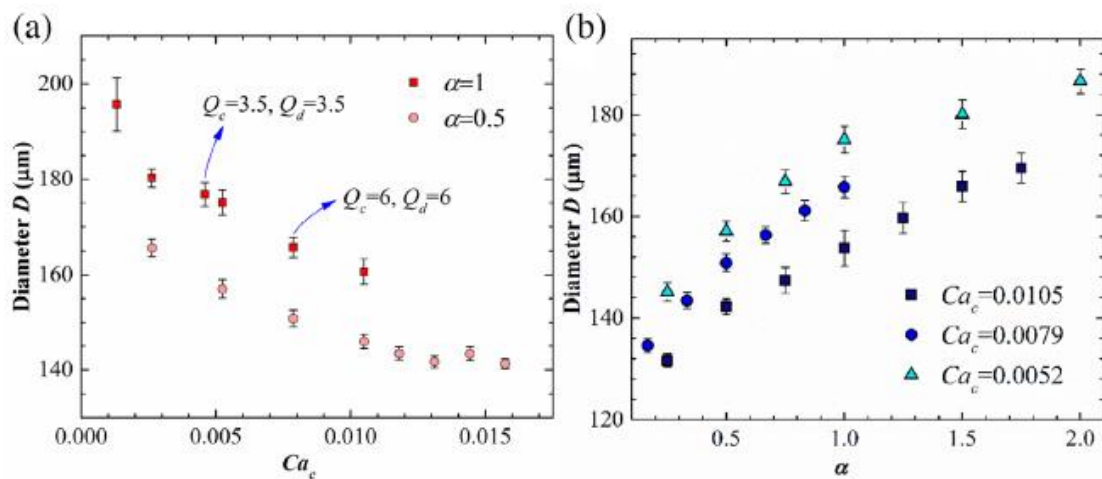


Fig. 2.2 Effects of the flow rate on droplet diameter depending on the Ca_c (a) and α (b) [1]

Several experiments under different flow conditions were performed, changing the velocity of both phases. It was proven that the flow rate ratio and the capillary number were the main factors that affected the droplet size. Furthermore, it was also concluded that under the same flow rate ratio, the droplet diameter was reduced by the increase of the Capillary number of the continuous phase. And in addition, the droplet size increased with the flow rate ratio (see Fig. 2.2).

As in a normal T-junction, the overall drop volume resulted from the sum of the volume of the filling stage (V_{fill}) and the one from the squeezing stage (V_{sq}). Moreover, the separation of stages was essential in order to understand the evolution of V_{fill} and the time of the squeezing stage (t_{sq}) along the flow rate ratio.

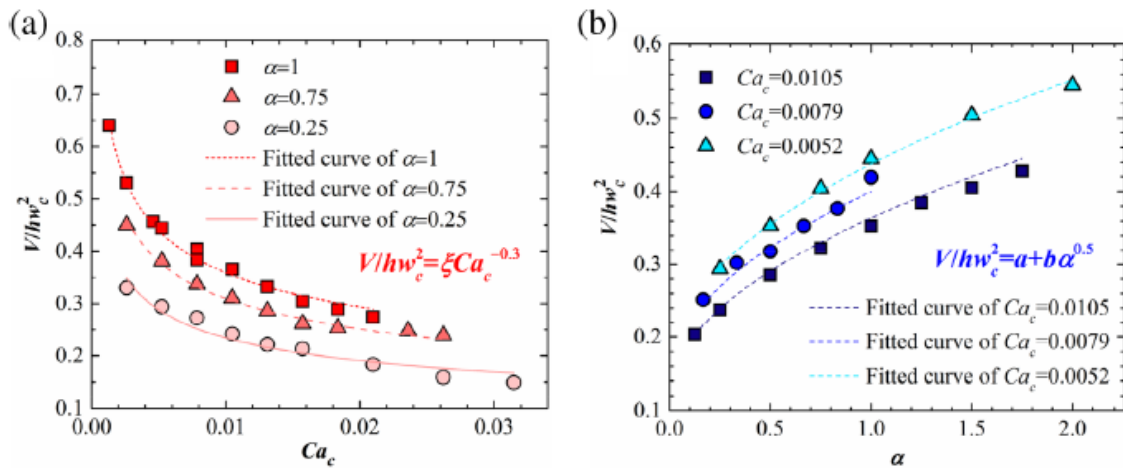


Fig. 2.3 Normalized droplet volumes of experiments and their fitted curves varied with the Ca_c under uniform flow rate ratio α (a); α under uniform Ca_c (b) [1]

In the filling stage, V_{fill} depends on the flow rate ratio and increases for cases under the same total flow rate while it fluctuates around average size. To sum up, they concluded that even though the flow rate ratio was the same, the thread shape and the droplet size varied when the flow rate was different.

Even though, in the squeezing stage, they stated that t_{sq} increased with the flow rate ratio for a uniform total flow rate but decreased for a uniform flow rate of the continuous phase. So, both continuous and dispersed flow rates have effects on the t_{sq} and, consequently, on V_{sq} (see Fig. 2.3).

Finally, a model to predict the droplet volume was determined. So, analysing all the data collected during the experiments, plotting some graphics and establishing some constants, they successfully created an equation with a less than 10% deviation of the results to predict the droplet volume.

A good predictive model using the fitted curves was achieved but it had no physical meaning. Until it was thought that using all the equations obtained during

the experiments, the droplet volume varied with the flow rate ratio α and the Capillary number Ca_c , providing the physical meaning they were lacking.

The paper concluded with a summary of the different ideas they extracted from all the experiments. The main goal, which was to create a predictive model for the size of the droplets in a T-junction with a neck, was achieved and validated. However, they also determined that the droplet volume was highly influenced by the Capillary number and the flow rate ratio. They additionally defined that the droplet generation can be divided into two stages regardless of the generation regime, which depends on if the cap of the dispersed phase thread can arrive at the opposite wall.

Once the summary of the text has been done, it is interesting to specify all the parameters that are going to be the same as in the paper and also the plots that are going to be reproduced in this study with the different data that will be taken from it.

The geometry, both of the liquids used and their velocities will be the same. The main graphics that are going to be reproduced are Fig. 2.2 and Fig. 2.3 that analyse the diameter and the volume of the droplets, as well as, a comparison of the experimental and the simulated data. In order to calculate the volume of the droplets, the same formula is going to be used, which can be seen in Eq. 4.1 in Chapter 4.

2.2. Problem statement

Here, the fluid properties of both liquids will be clarified and the most important dimensionless numbers of the fluid mechanics will be explained and calculated, in order to have a more accurate physical visualisation of what is happening inside the T-junction.

2.2.1 Fluid characteristics

As was mentioned before, for this experiment there will be two phases and, therefore, two liquids; the dispersed phase which is deionised water will have the sub-index “d” and the continuous phase flowed, which is sunflower oil will have the “c”.

In the scientific article [1] the temperature was not specified, as the parameters were measured at the moment, therefore standard temperature will be assumed, which is 25°C.

In table 2.1, viscosities and densities at the chosen temperature can be seen. The dynamic viscosities were taken from the paper, the densities for the water [16] and sunflower oil [15] were looked up and the kinematic viscosities were calculated using the following Eq. 2.1. It is true that density of water at 25°C is

not exactly 1000 kg/m³, however to have more rounded numbers for the kinematic viscosity, this approximation will be done.

$$\gamma = \frac{\mu}{\rho} \quad (2.1)$$

Where γ is the kinematic viscosity, μ is the dynamic viscosity and, finally ρ is the density.

Table 2.1 Fluid properties values

<i>Fluid properties</i>	<i>Dynamic viscosity [kg/m·s]</i>	<i>Density [kg/m³]</i>	<i>Kinematic viscosity [m²/s]</i>
<i>Water (d)</i>	1.01 · 10 ⁻³	1000	1 · 10 ⁻⁶
<i>Oil (c)</i>	47.2 · 10 ⁻³	918.8	5.14 · 10 ⁻⁵

Dynamic viscosity is necessary because the software OpenFOAM uses it, instead of kinematic viscosity when setting up the parameters for the simulations. This in depth explained in Appendix A.1. Finally, the last parameter that has to be taken into account is the surface tension, $\sigma = 30.1 \text{ mN/m}$, which is taken from the article.

In the scientific paper, they used several injection velocities for both of the phases that vary in the range of 0.5 to 24 $\mu\text{l/min}$. However, the range numbers used in this project are between 8 and 1 $\mu\text{l/min}$, depending on the fluid and the simulation. All velocities were calculated using Eq. 2.2 and the flow rate ratio (α) with Eq. 2.3. It is important to calculate α because in the article it is used several times and it will be one of the main parameters used taken into account in the comparisons done for the results in Chapter 4.

$$U = \frac{Q}{A} \quad (2.2)$$

$$\alpha = \frac{Q_d}{Q_c} \quad (2.3)$$

Where U would be the velocity, Q_c and Q_d are the volumetric flow rates for sunflower oil and water, respectively; and A is the cross-sectional area of the capillary.

2.2.2 Context verification

In fluid mechanics, dimensionless numbers are really useful in order to determine the flow characteristics of a fluid [17]. As this experiment is performed in a microgravity environment, the fluid system is dominated by surface forces instead of body forces, making gravity and density effects negligible for fluid handling [10]. Therefore, it is important to study and verify that the forces associated to the different dimensionless numbers are the ones that should be acting in this context.

In this sub-chapter an analysis of the most important dimensionless numbers that take part in this type of experiment is going to be done. Being the Reynolds number, the Capillary number, the Bond number and the Weber number the most important ones, as well as, the ones that are going to be studied. In table 2.2 a compilation of the results for all the calculations can be seen.

The first one it is going to be described is the Reynolds number which is the ratio between inertial and viscous forces [18]. In this experiment, it is important because the effect of viscosity is crucial when controlling the velocities of the fluids. Once the computation has been done, it can be determined if the flow is laminar or turbulent, depending on the result. If it is greater than 2900, it is turbulent, but if it is smaller than 2300 it is laminar. The next Eq. 2.4 shows how it can be calculated.

$$Re = \frac{\rho \cdot U \cdot L}{\mu} \quad (2.4)$$

Where the ρ is the density of the fluid in kg/m^3 , U is the flow speed of it in m/s, μ is the dynamic viscosity in $kg/m \cdot s$ and L is the characteristic length, which in a rectangular duct can be expressed as the hydraulic diameter D_H and should be calculated as seen in Eq. 2.5 [19]. The parameter A corresponds to the cross sectional area of the flow and P to the wetted perimeter, which would be the perimeter because all the duct is filled with oil. The exact dimensions of the channel can be seen in the paper or in the first sub-chapter of Chapter 3.

$$D_H = \frac{4 \cdot A}{P} \quad (2.5)$$

Yet another dimensionless quantity that is essential and has been mentioned before several times is the Capillary number [20]. This one represents the relative effect of viscous forces versus surface tension forces, in this case, two immiscible liquids, water and sunflower oil. If the result is $Ca \ll 1$ [33], the flow is dominated by capillary forces, whereas if it is greater, the viscous forces are the prevailing ones. It could be calculated using Eq. 2.6, where the μ and U are the dynamic viscosity and fluid velocity, respectively, and σ is the surface tension.

$$Ca = \frac{\mu \cdot U}{\sigma} \quad (2.6)$$

However, in the paper, there is another formula (see Eq. 2.7) that can be used to calculate the Capillary number for the continuous phase, which is essentially the same one but adapted to the continuous phase and replacing U for $Q_c/h \cdot w_c$. Not only that, as it depends on the fluid velocity and the range of velocities used is between 0.5 and 24 $\mu\text{l}/\text{min}$, there is also a range of values where the calculated Capillary number must be in which is 0.0026 and 0.031.

$$Ca = \frac{Q_c \cdot \mu_c}{h \cdot w_c \cdot \sigma} \quad (2.7)$$

As can be seen in table 2.2, the values calculated are between the correct range of values. Therefore, it is possible to say that the computation of this dimensionless number is accurate.

Considering this experiment is performed in microgravity conditions, it would be quite interesting to consider the significance of the Bond number, also known as the Eötvös number (Eo) [21], in order to check the importance of the gravitational forces compared to surface forces. The result should be lower than 1, which indicates that surface forces are dominant and that the gravitational ones can be neglected. The equation to calculate it is Eq. 2.8.

$$Bo = \frac{\Delta\rho \cdot g \cdot L^2}{\sigma} \quad (2.8)$$

Where $\Delta\rho$ is the difference between the density of both liquids, g is gravity, σ is the surface tension and L is the characteristic length, which could be, for example, the radius of one of the droplets or the diameter of the capillary. However, in this case, it is going to be the same as the one for the Reynolds number, calculated in Eq. 2.5.

Finally, the last number that will be mentioned is the Weber number [22] which is useful when there is an interface between two immiscible liquids which also have curved surfaces. It is the ratio between inertia force and surface tension, therefore if the weber number is smaller than 1, surface tension is predominant, which is what it is aimed for Eq 2.9 shows the formula used to do the calculations for this dimensionless number.

$$We = \frac{\rho \cdot U^2 \cdot L}{\sigma} \quad (2.9)$$

As in the previous equations, ρ is for density, U for velocity and σ for surface tension. Here the characteristic length L will be determined as before in Eq.2.5.

Once all dimensionless numbers have been presented and calculated, they are shown in table 2.2, with the maximum and minimum values respectively, achieved during all the experiments depending on the different velocities and on the phase.

Table 2.2 Maximum and minimum dimensionless numbers values

<i>Phases</i>	<i>Value</i>	<i>U [m/s]</i>	<i>Re</i>	<i>Ca</i>	<i>Bo</i>	<i>We</i>
<i>Continuous</i>	max	0.0067	0.0174	0.0105	0.0005	0.0002
	min	0.0017	0.0044	0.0026		0.00002
<i>Dispersed</i>	max	0.0133	1.7558	0.0005	0.0005	0.0008
	min	0.0033	0.0436	0.0001		0.00005

To sum up, looking at the obtained results it is possible to say that we are working with a laminar flow, that the gravitational forces are negligible and that capillary forces are dominant over inertial forces, but at the same time, viscous forces are dominant over inertial forces, as expected for this type of experiment. These calculations have verified the environment where the simulations are going to be performed, as well as, giving a better idea of the different forces acting in the T-junction.

2.2.3 Contact angle

A very important parameter that is going to have a huge impact in the outcome of the simulations is the contact angle.

The contact angle can be defined as the angle a liquid creates with a solid or liquid when it is deposited on it. Their properties and the interaction and repulsion forces between them will determine the angle. Those interactions are described by cohesion and adhesion forces. So, the balance between the cohesive forces of similar molecules, such as between the liquid ones; and the adhesive forces between non-similar molecules, for example between the liquid and the solid ones, will determine the contact angle created [23].

Using this contact angle, it is possible to measure the wettability of a surface or material. A wetting liquid is one that forms a contact angle smaller than 90° with the solid and it will be considered hydrophilic. Therefore, a non-wetting liquid creates a contact angle between 90° and 180° , consequently, this one will be hydrophobic.

Even though the contact angle is specified in the paper as 165° , it will have to be adapted in order to replicate the experiments in the simulations, because in OpenFOAM, the determination of the contact angles is completely different due to the fact that it is measured through the oil instead of through the water. Therefore, the angles that will be used in this project are smaller than 90° in order to be hydrophobic and create the droplets that are looked for.

In Fig. 2.4 all the terms described before can be seen. This sketch shows the evolution of the contact angle for each of the types of wettability. The first one shows a super hydrophobic and non-wetting material with a droplet formation, which is exactly what it is aimed for the droplets of this experiment. This is why in the paper the angle used will be greater than 150° and in OpenFOAM it will be around 30° .

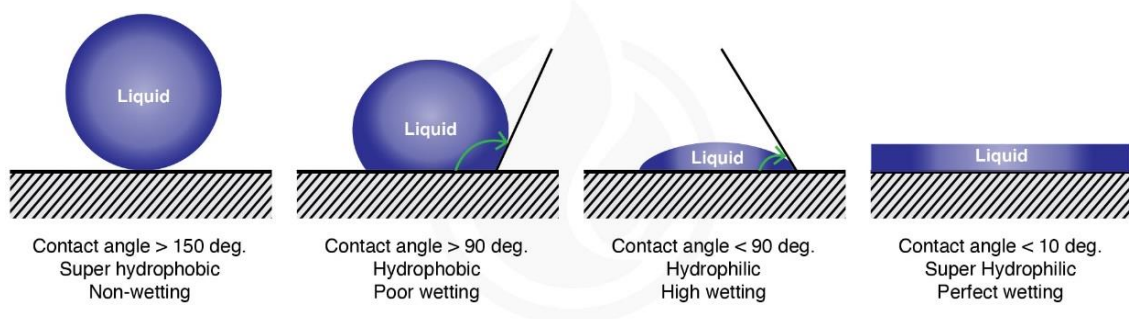


Fig 2.4 Description of the contact angle [24]

2.3 Methodology: CFD

Computational Fluid Dynamics (CFD) is a branch of the science of fluid mechanics that, with the help of computers, produces quantitative predictions of fluid-flow phenomena using numerical analysis and data structures [25].

It can be said that CFD is seen as a group of computational methodologies used to solve equations governing fluid flow. First of all, it is critical to define the boundary conditions of the problem and then, to decide which set of physical assumptions and related equations need to be used for the problem at hand. Several laws and equations can be used: conservation laws, continue conservation laws, compressible and incompressible Navier-Stokes equations and Euler's equations, among many others.

Computers are used for the calculations required to simulate the flow, so the better the computer, the better the result obtained. With high-speed supercomputers, better solutions can be achieved, even though the predictions are never completely exact. This method is handy when previously performing an analytical or empirical analysis of a particular problem because it can be used for comparison, which is exactly this case.

CFD can be used in many fields of study and industries, which could include aerodynamics and aerospace analysis, weather simulations, industrial system design, biological engineering, visual effects for films and video games and combustion analysis, to give some examples [26].

A basic procedure to follow when performing this type of simulation includes different stages: pre-processing (see subchapter 2.3.1), simulation (see subchapter 2.3.2) and post-processing (see subchapter 2.3.3), which will be explained in depth in the following sub-chapters.

In Fig. 2.5 a 2D CFD simulation performed in *Ansys* can be seen. It shows an analysis of the velocity field around an airfoil. The different colours show the different velocities around it.

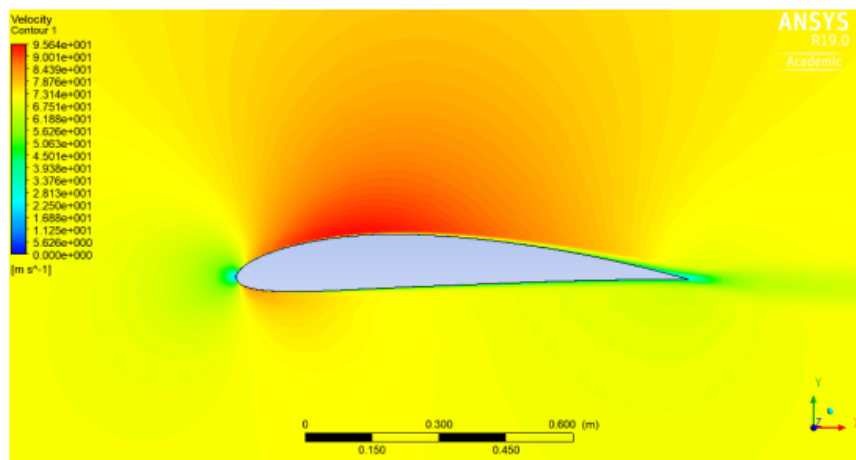


Fig. 2.5 CFD analysis of velocity field around an airfoil [27]

2.3.1 Pre-processing

In the pre-processing part, the geometry and the physical bounds of the problem must be defined using a computer-aided design (CAD) to, later on, divide it into discrete cells in order to create a mesh. This part was done using the software *Ansys* due to its easy-to-use and free platform, as well as, the possibility to export it into a compatible format with OpenFOAM to do the simulations afterwards. The boundary conditions, fluid behaviour and properties must also be chosen in this part which will be specified using the software OpenFOAM.

In Fig. 2.6 an image from the scientific paper showing the geometry they used can be seen and in table 2.3 the dimension of each parameter.

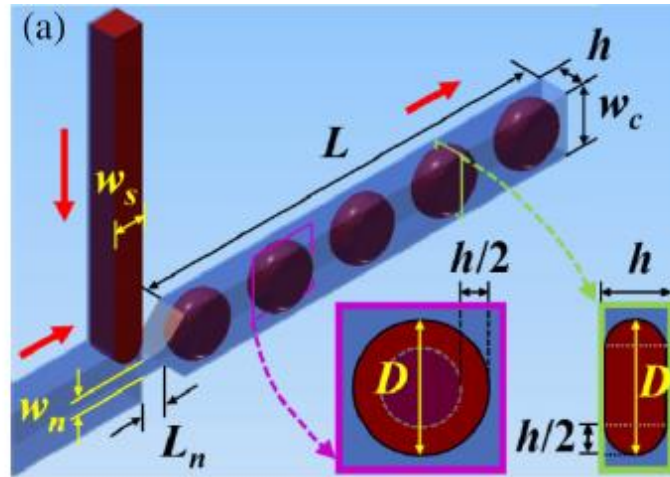


Fig. 2.6 Geometry used in the scientific paper [1]

Table 2.3 Dimensions of the T-shape channel with a neck

<i>Parameters</i>	w_c	w_s	w_n	L_n	h
<i>Dimensions [μm]</i>	200	100	60	60	100

The geometry for the simulations showing the dimensions can be seen in Fig. 3.1 in the following chapter. It can be appreciated that the longitude of the channel is not specified, but in the following chapter it will be indicated and justified.

In Fig. 2.7, the geometry for the simulations can be seen, as well as its different boundaries. Through inlet1 flows oil, through inlet2 flows water and through the outlet the mixture of both. Each number represents the wall's number, for example, 1 would represent wall1, 2 represents wall2 (the back one) and so on until thirteen.

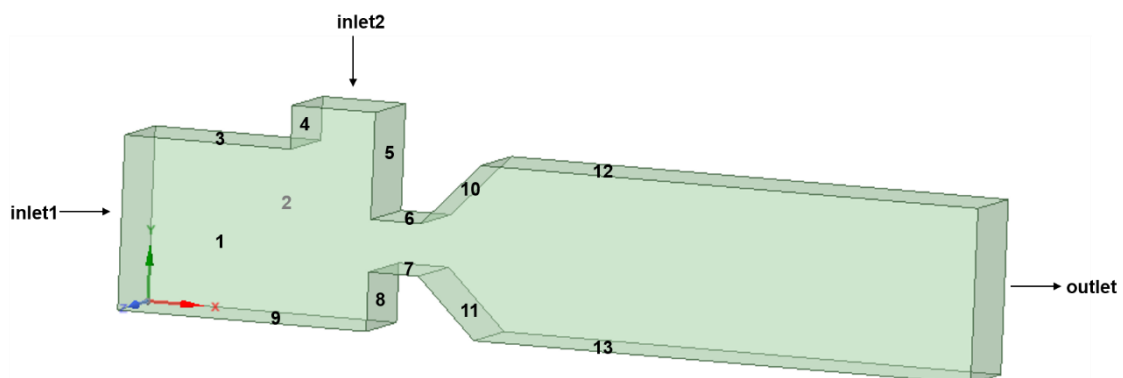


Fig. 2.7 Geometry with its boundaries

After the geometry is created, the type of mesh must be chosen and done. This mesh will have to be exported as a .msh file and converted to OpenFOAM, using the *fluent3DMeshToFoam* command, for the purpose of being able to use it. It has to be mentioned that to be compatible with OpenFOAM it is necessary to name all the sections and write exactly the same name it is going to be used in the files because if not, it will not work properly. However, as it changed several times during the simulations, they will be presented in Chapter 3, showing as well the criteria followed to change it every time.

Another important step is to define the initial conditions of the simulation. The three main parameters that will be settled are the velocity, pressure and oil fraction, which will be, as well, showed in depth in the first part of Chapter 3. In the oil fraction file both phases for the fluids have to be set, which in this case will be $\alpha = 1$ for oil and $\alpha = 0$ for water.

For the velocity, it will be stated that at initial time, both of the fluids have zero velocity. The internal field of pressure will be as well at zero. Finally, for the oil fraction it will be set as the entire geometry is filled with oil and water starts running through it.

2.3.2 Solver

The simulations will be performed using the software OpenFOAM and a multi-core computer from the EETAC which will make the simulations much faster.

The chosen program to perform the numerical simulations was OpenFOAM (for Open Field Operation and Manipulation) which is a CFD software, completely free and open-source [28]. It has several features to simulate from turbulent flows to scenarios involving chemical reactions, but not only that, it includes tools for meshing around complex geometries and for data processing and visualisation. Furthermore, it allows the users to perform these simulations in parallel, in order to take advantage of the multi-core processors and multiprocessor computers.

One of its main advantages is that it has no license costs, so it is completely free, but additionally, it gives the opportunity to analyse systems and conditions which are very difficult to simulate experimentally. However, there is no interface, therefore it is quite difficult to use and requires several weeks of training before getting into the user's experiment. OpenFOAM simulations are configured by several plain text input files, in C++ language, located across the following three directories (see Fig. 2.8). Additional text files can be generated, but these are the ones used in the simulation.

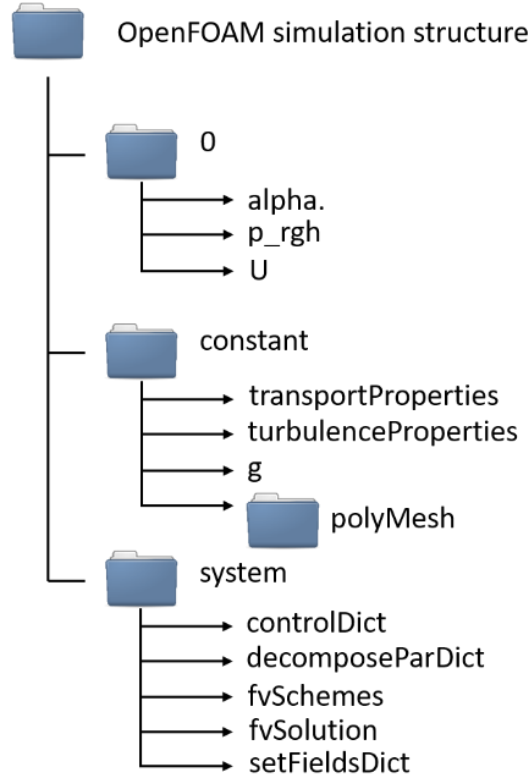


Fig. 2.8 Overview of the OpenFOAM software directory structure used

As we can see in Fig. 2.8, the basic structure of an OpenFOAM directory consists of three main folders: 0, constant and system. The 0 folder contains the files regarding time directories, so it is named “0” because it is at the initial time and, in this case, it would indicate the initial conditions for the experiment. The “constant” folder contains information regarding mesh and the files that specify the physical properties of the fluids. Finally, the “system” folder sets the parameters associated with the solution procedure itself. For more details on the different files or an example of each of them, see Appendix A.1.

When using OpenFOAM different solvers can be chosen and for this type of experiment the best one is InterFOAM, which is a two-phase solver for incompressible, isothermal and immiscible fluids which uses the volume of fluid concept (VOF). It solves the Navier-Stokes equations for the fluids meaning that the material properties are constant in the region filled by one of the two liquids except at the interface. It uses the continuity equation (Eq. 2.10), the momentum equation (Eq 2.11) and what is called the conservation of the mixture components along the path of a fluid parcel (Eq. 2.12) [31].

$$\frac{\partial u_j}{\partial x_j} = 0 \quad (2.10)$$

$$\frac{\partial(\rho u_i)}{\partial t} + \frac{\partial}{\partial x_j}(\rho u_j u_i) = -\frac{\partial p}{\partial x_i} + \frac{\partial}{\partial x_j}(\tau_{ij} + \tau_{t_{ij}}) + p g_i + f_{\sigma i} \quad (2.11)$$

$$\frac{\partial \alpha}{\partial t} + \frac{\partial(\alpha u_j)}{\partial x_j} = 0 \quad (2.12)$$

Where u is the velocity, g_i is the gravitational acceleration (which would be zero in this case), p is the pressure, $f_{\sigma i}$ is the surface tension and τ_{ij} and $\tau_{t ij}$ are the viscose and turbulent stresses respectively.

The EETAC cluster was mainly used to minimize the computational time of the different simulations by splitting it into different cores (with a maximum of 7). At the file *decomposeParDict*, the chosen method for the decomposition is determined, which is the *scotch* method. For the purpose of choosing the number of cores in which the simulation had to be divided, a number of cores trial was done.

Table 2.4 Simulation time depending on the number of cores

<i>Number of cores</i>	<i>Clock time [s]</i>	<i>Real-time [h]</i>
1	13456	3.73
4	4170	1.16
6	4056	1.13

As can be seen in table 2.4, the optimum number of cores used is 6, which is the number of cores that perform the most efficient simulation and is the number of cores that will be used around the project in order to perform the simulations as fast as possible.

2.3.3 Post-processing

Finally, the post-processing part will be essentially done with the software ParaView which is an open-source, multi-platform data analysis and visualization application. After that Excel will be used to collect the data and plot some graphics in order to compare the results between the experiments of the paper and the simulations performed.

As ParaView is integrated with OpenFOAM, both are completely compatible and this allows to see the results simulated easily. It also includes many tools, however, for this project, only a few will be used such as the slice one, to see the interior of the geometry or the ruler one, to measure the different droplets generated. For a further explanation of the ParaView software, check Appendix A.3.

In Fig. 2.9 an example of the formation of a droplet in the paper's experiment, at $Q_C = Q_D = 6\mu\text{l}/\text{min}$ can be appreciated. It is possible to see the evolution of the droplet at the different times and, a comparison can be done looking at both figures, Fig. 2.9 and Fig. 2.10.

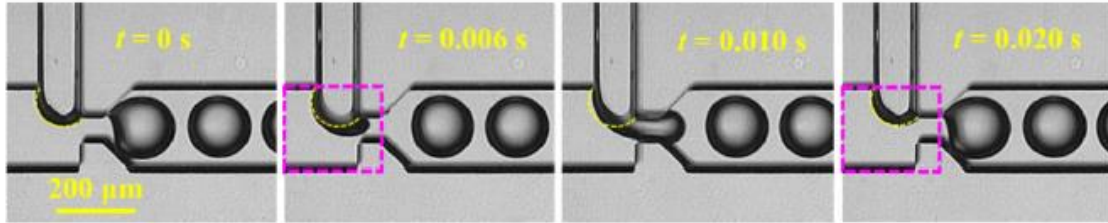


Fig. 2.9 Dynamics of droplet formation and droplet size in the T-junction with a neck [1]

In Fig. 2.10, an example of the visualization of a simulation can be seen. The colour red represents the continuous phase (oil) and the blue one represents the dispersed phase (water) forming the different droplets. The interface is the zone between the two liquids and it is shown in white colour. At the right bottom part of the image the scale can be seen, showing that the continuous phase which is oil correspond to $\alpha = 1$ and the dispersed phase, water, to $\alpha = 0$.

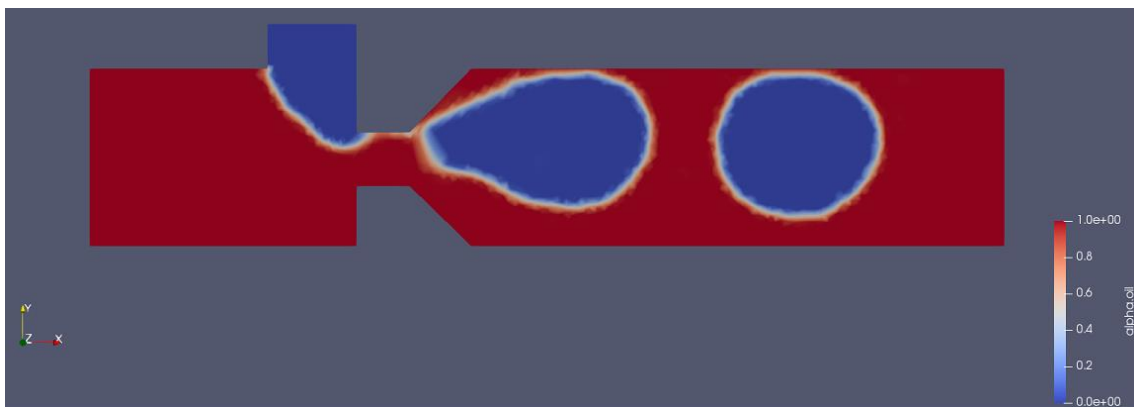


Fig. 2.10 Example of a simulation with $Q_C = Q_D = 6\mu\text{l}/\text{min}$

CHAPTER 3. EVOLUTION OF THE SIMULATIONS

Once all the context of microfluidics and microgravity has been specified and the fluids presented, it is time to explain how the simulations evolved during this time. Throughout this project, there has been a progression of the simulations performed, and there has been a huge change between the first and the last one. Some parameters have been improved, such as the geometry, mesh, boundary conditions and contact angle, among others.

3.1 Early stages

The project began with the reading and understanding of the paper [1] summarized before, as well as the investigation and comprehension of some of the topics mentioned, like microgravity, microfluidics and droplet-based microfluidics.

Once this was done, there was a period of time that involved the familiarization with the tools that were going to be used, for instance, OpenFOAM for the simulations, and *Ansys* for the geometry and mesh. After looking up some tutorials and practising for a short time, the first geometry could be made following the description in the paper, as can be seen in Fig. 3.1.

It has to be mentioned that the longitude between inlet1 and the start of the neck was not specified and it was decided to be this long because it gives the droplet enough space to form, without adding unnecessary simulation time. It is possible to say the same about the longitude between the end of the neck and the outlet, giving the droplet enough time to form and stabilize.

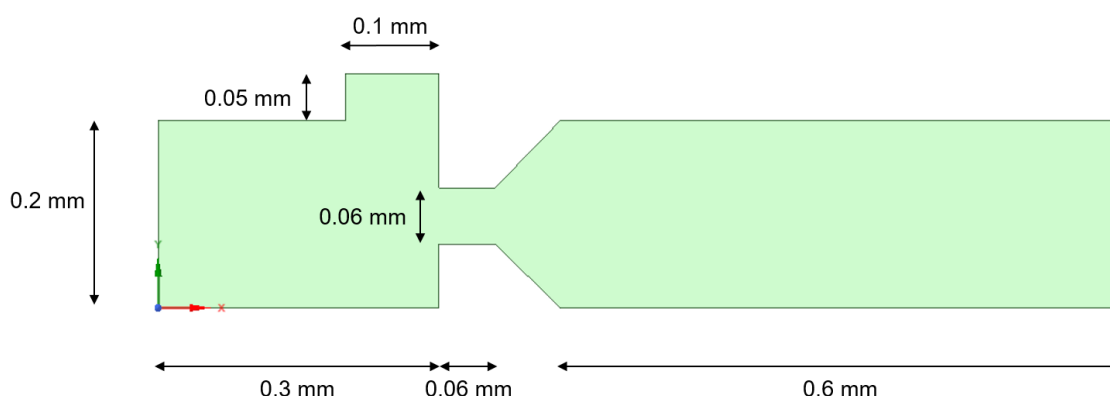


Fig. 3.1 Basic geometry for the simulations and dimensions.

As we can see in Fig. 3.1, the geometry consists of a T-junction with a neck where two rectangular capillaries meet at a 90-degree angle, resulting in just one outlet.

The depth of the channels is 0.1mm and as the length of the channel was not specified in the paper, so it was decided to be 0.6mm. Through inlet1 the oil runs and through inlet2, water, resulting in one outlet with the oil-water mixture.

However, in order to decide the boundary conditions faster, as well as making the simulations take less time, it was determined that the geometry would be much simpler at first, only involving its critical parts, which are the two inlets, the neck and the outlet, as can be seen in Fig. 3.2.

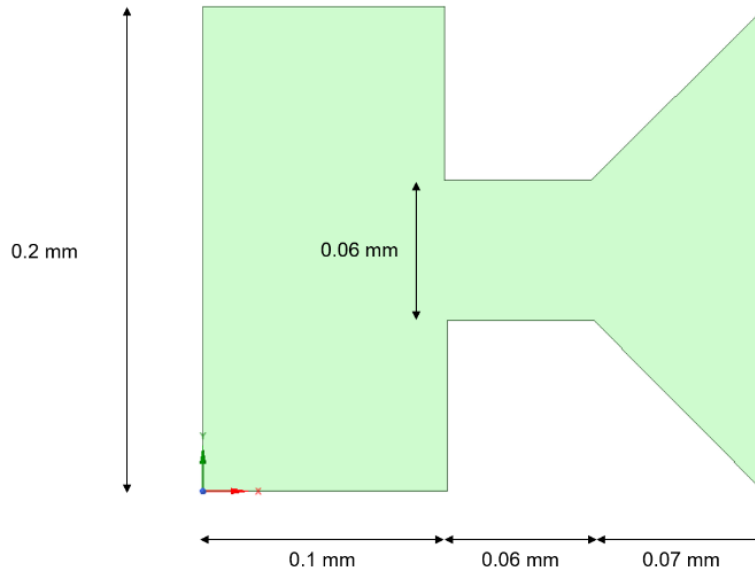


Fig. 3.2 First geometry for the initial simulations and dimensions.

As soon as the first geometry was done, it was time to decide how would the mesh be. It was decided that it had to be denser at the top parts in order to see the formation of the droplet better, as well as seeing the neck more clearly, as can be appreciated in Fig 3.3, but at the same time it was required to be quite simple.

The first mesh created can be seen in Fig. 3.3, which is a tetrahedral mesh with inflation (a part with a higher density of cells) in 4 of the walls. In specific, this mesh has a total of 56 731 cells and has these characteristics:

- Type of mesh: CFD compatible, fluent, linear with a tetrahedral method and patch conforming algorithm.
- Body sizing: the element size is $7.5 \cdot 10^{-6}$ m.
- Inflation: 15 layers with a growth rate of 1.2 and maximum thickness of $1 \cdot 10^{-4}$ m.

After the mesh and geometry were created and exported as mentioned in the previous chapter (Chapter 2.3.1), it was time to start working with OpenFOAM.

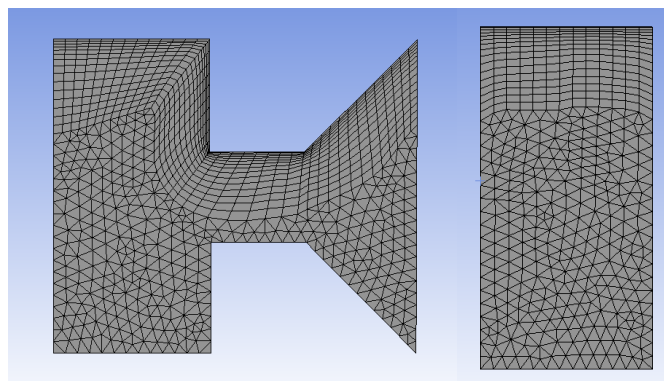


Fig. 3.3 First mesh for the first geometry

The basic files could be taken from one of the many tutorials the software has for the users in order to practice, but specifically, the files located in *multiphase*, *InterFOAM*, *laminar* and *capillaryRise*. It has to be remarked that very important and useful references were found in a similar project Carlos Moreno did a couple of years ago [32]. In addition, for more detail on a certain file from the simulations or just more information about the meaning or content, check Appendix A.1 regarding the case folder of OpenFOAM.

In order to adapt the already existing files to this particular experiment, several changes had to be made. Some of the files were changed once and remained untouched until the end of the simulations. However, some others were changed many more times for the purpose of finding the most accurate solution that validated the experiment of the paper, such as the files containing the boundary conditions or the velocity.

As a starting point, the boundary conditions can be found in the following tables. The actual geometry has a total of 12 boundaries at first (two inlets, one outlet and 9 walls) and there are 3 different fields (oil fraction, velocity and pressure).

To sum up, the total number of boundary conditions would be 36, but in order to explain it better, the walls will be treated as one. Even though for each wall there is a different boundary condition, depending on where is it located and if it receives water contact or not.

Table 3.1 Review of the boundary conditions in the alpha file.

<i>Boundary</i>	<i>Condition</i>	<i>Value</i>
<i>Inlet1</i>	inletOutlet	uniform 1
<i>Inlet2</i>	inletOutlet	uniform 0
<i>Outlet</i>	zeroGradient	-
<i>Walls</i>	constantAlphaContactAngle	uniform 1

As can be appreciated in the table 3.1 for the alpha file, the *inletOutlet* conditions basically set the reverse flow to a fixed value which, in this case, would be 1 or 0 depending on the inlet (1 for oil and 0 for water), *zeroGradient* condition sets the field to the internal field value, which would be 1 in this case because the capillary is filled with oil and *constantAlphaContactAngle* sets a constant angle at the different walls of the channel. So, depending on the type of wall the angle would be one or another with values from 0 to 180, as explained in Chapter 2.2.3 for the contact angle.

Table 3.2 Review of the boundary conditions in the pressure file.

<i>Boundary</i>	<i>Condition</i>	<i>Value</i>
<i>Inlet1 and Inlet2</i>	zeroGradient	-
<i>Outlet</i>	fixedValue	$\$internalField$
<i>Walls</i>	fixedFluxValue	$\$internalField$

Table 3.2 shows the pressure file, inlet1 and inlet2 have the same conditions as before, when the *zeroGradient* one was being used. Therefore, the pressure gradient is set to 0, which is the same as the internal field value. At the outlet, the pressure is set to a *fixedValue*, the same as the internal field which is 0. Finally, using the *fixedFluxPressure* condition the pressure gradient is adjusted, so that the flux at the boundary is specified by the velocity boundary condition which will be 0 as well.

Table 3.3 Review of the boundary conditions in the velocity file.

<i>Boundary</i>	<i>Condition</i>	<i>Value</i>
<i>Inlet1</i>	fixedValue	uniform (0.005 0 0)
<i>Inlet2</i>	fixedValue	uniform (0 -0.01 0)
<i>Outlet</i>	pressureInletOutletVelocity	$\$internalField$
<i>Walls</i>	fixedValue	$\$internalField$

Lastly, as seen in table 3.3 for the case when $Q_C = Q_D = 6\mu\text{l}/\text{min}$, it can be appreciated that in inlet1, the oil will be injected at a constant velocity of 0.005 m/s at the x-axis direction and in inlet2 water will be injected at a constant velocity of -0.01 m/s at the y-axis direction. At the walls, the no-slip condition is applied by setting the value of the internal field which is 0. The outlet has the *pressureInletOutletVelocity* condition which means that for the flow out of the domain the *zeroGradientCondition* is set and for the flow inside it, the velocity is assigned based on the flux.

These were the basic boundary conditions used for the simulations, however, the only ones that were changed were the contact angle for the different walls, having a variation every time a simulation was performed. In order to see the contact angle used for every final simulation from where the plotted data was taken see Appendix C.2.2.

What was aimed for this firsts simulations, was to try to get one where its boundary conditions made the fluids act like in the paper and in the same amount of time.

For example, the simulation shown in Fig 3.5 tries to follow the same stages that Fig. 2.1 shows, which can also be seen more clearly in Fig. 3.4, for the same velocity, which is $Q_C = Q_D = 6\mu\text{l}/\text{min}$. Actually, it is not completely accurate because in the simulations at time 0s, water starts to run through inlet2, whereas in the paper, at time 0s the fluid is as in the first picture of Fig. 3.5.

Even though, it can be seen that in the paper the experiment takes 0.018s until the breakup stage begins, while in the simulation it takes approximately 0.0184s, which is a quite accurate simulation.

Nevertheless, the amount of time that each stage takes can also be compared; for instance, in the paper, the filling stage takes 0.008s to complete and 0.01s for the squeezing stage, while in contrast, if the simulations are checked closely, the filling stage takes approximately 0.0064s and the squeezing stage takes 0.012s.

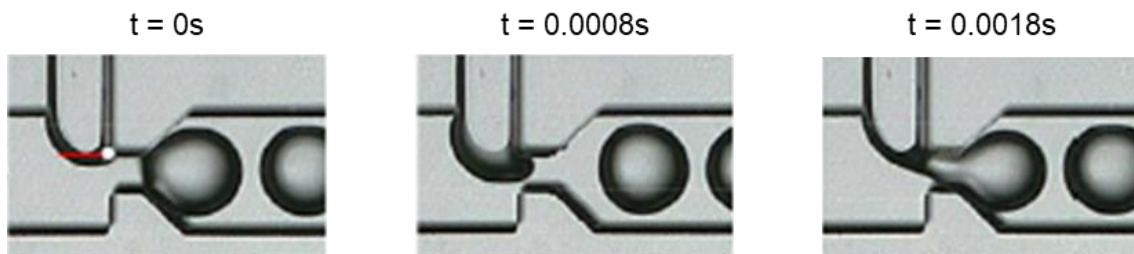


Fig. 3.4 Experimental droplet generation period with its time steps [1]

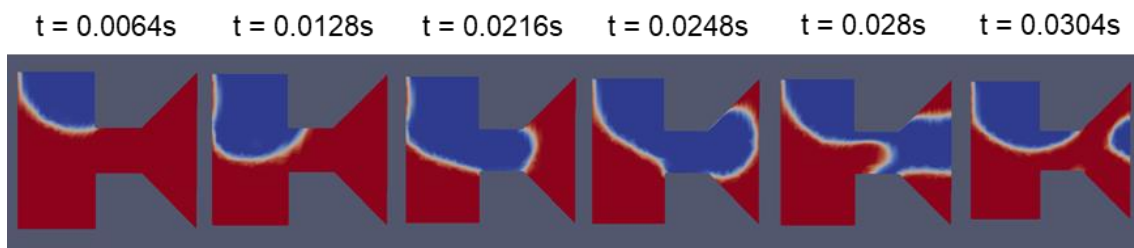


Fig. 3.5 Evolution of the droplet formation in the simulation for the boundary conditions chosen

Overall, it can be said that the simulations and the boundary conditions were good enough and the simulations performed gave valid results, just when analysing the timings of these two stages. As it is a greatly small geometry it was not possible to check the diameter nor the volume, since the complete droplet was not possible to be seen.

In consequence, it was decided to continue and expand the geometry in order to see if they worked for different geometries or not. Additionally, it was necessary to start increasing the geometry, until it was more like the one in the experimental paper, as well as refining the mesh because as can be seen in the image, the interface between water and oil is quite thick. This analysis is going to be in depth explained in the following part of Chapter 3 where the fundamental part of the probing is performed in order to try to find the perfect boundary conditions that perform the simulations as accurately as possible.

It has to be pointed out that for the simulations, the EETAC cluster was supposed to be used, but as the instructions given were not quite clear and it was difficult to use, this tool was not utilised for these first tests. However, for the following ones, it will be used and it will also be essential in order to perform the simulations nicely.

To have an idea of the proportion of this first part, about 30 simulations were performed until finding the one mentioned before, taking approximately 120 hours to run in total.

3.2 Fundamental probing

During this stage of the project, a new geometry with new and different meshes was tried along with several boundary conditions to make the simulations as errorless as possible.

3.2.1 Mesh definition

The next step that was followed was changing the geometry, making it a bit bigger, specifically, the channel between the neck and the outlet increased by 0.2mm, as can be seen in the following Fig. 3.6. This second geometry allowed the droplet to form and it made possible as well to measure the volume and the diameter of the droplet, even though the droplet was not stabilized completely due to the lack of space.

When doing the second geometry, several tests were run in order to compare it with the old one, in order to see if the results got better or not. The majority of these analyses consisted in changing the mesh and comparing the results to the ones performed before.

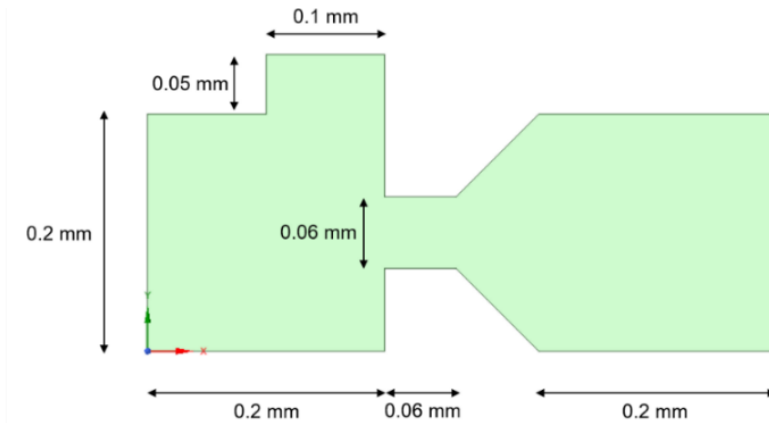


Fig. 3.6 Second geometry for the simulations with its dimensions

For the purpose of checking if the results got better, some measurements were done using the ruler tool in ParaView, so for a further explanation on how it is used, Appendix A.3 can be looked at.

To start up, the first mesh created had more or less the same amount of cells, specifically, it has 55 798. Despite this, some basic characteristics were changed, such as the size of each cell and the number of layers of the inflation because it seemed that in the previous mesh with 15, it was much denser at the walls, which was not necessary. This first mesh can be seen in Fig. 3.7 and the comparison simulation with the other geometry can be appreciated in Fig. 3.8.

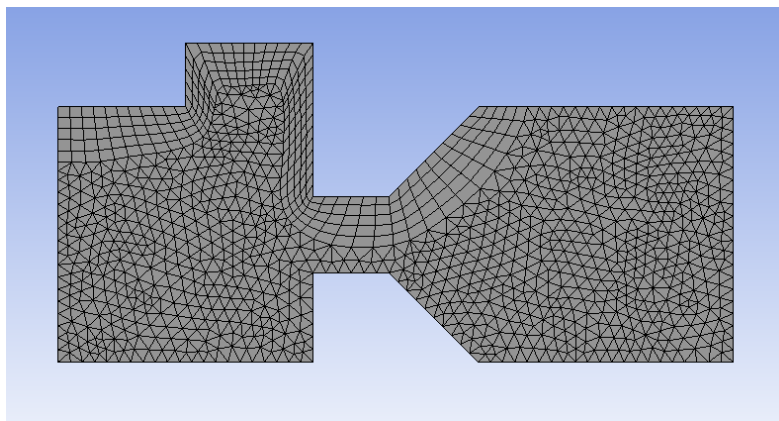


Fig. 3.7 First mesh for the second geometry

- Type of mesh: CFD compatible, fluent, linear with a tetrahedral method and patch-conforming algorithm.
- Body sizing: the element size is $9.5 \cdot 10^{-6}$ m.
- Inflation: 5 layers with a growth rate of 1.2 and a maximum thickness of $1 \cdot 10^{-4}$ m.

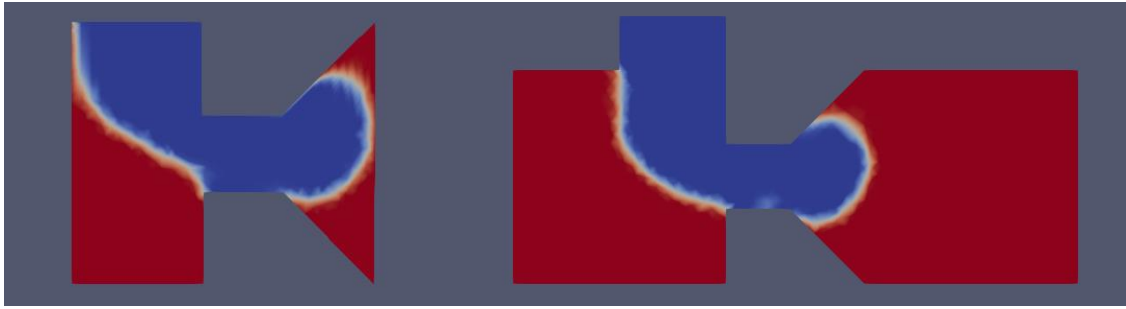


Fig. 3.8 Comparison simulation between the first and the second geometry with the same mesh

It can be perceived in Fig. 3.8 that the mesh used in the right simulation with the second geometry shows more blurred edges in the droplet. This could be happening because the same number of cells are being used in a much bigger geometry, therefore, the solution is way less accurate. For example, in the old geometry, this interface measures $1.77 \cdot 10^{-5} m$, while in the new one $2.74 \cdot 10^{-5} m$, which is a poorer result.

Once this first comparison was done, it was time to do another one to refine the mesh and see if a denser one was more useful than the last one. This new mesh has more or less twice the number of cells, particularly 119 651 cells. In order to be able to have more cells, the size of each one had to be reduced to $8.5 \cdot 10^{-6} m$, in spite of this, all the other mesh characteristics remained the same.

The second mesh for the second geometry can be appreciated in the following Fig. 3.9 and the comparison between the two simulations using the different meshes is represented in Fig. 3.10.

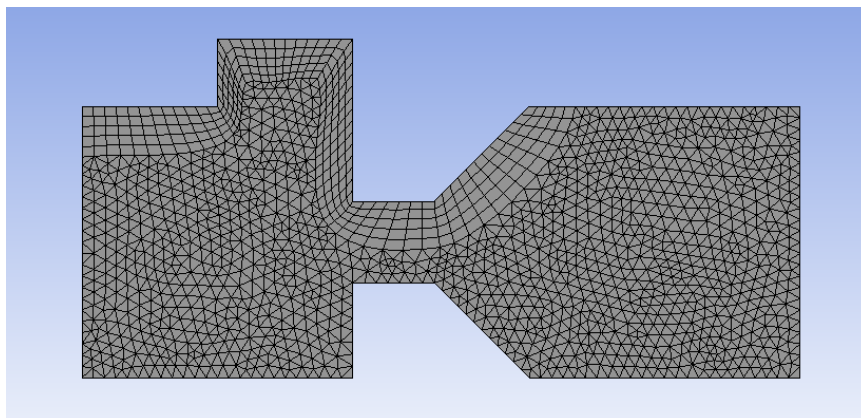


Fig. 3.9 The second mesh used for the new geometry

In Fig. 3.10 it can be appreciated at first sight, that the one on the right has very clear edges, just measuring $1.36 \cdot 10^{-5} m$, quite less than for the previous mesh, which was $2.74 \cdot 10^{-5} m$.

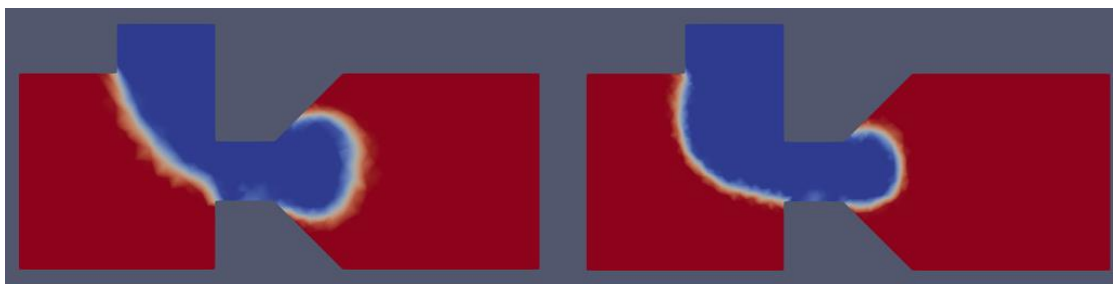


Fig. 3.10 Comparison simulation between the less dense mesh and a denser one

In table 3.4 a summary of the results obtained from the analysis between the meshes can be seen, showing the differences between the dimension of the interface. Consequently, this last mesh is the one that is going to be utilised from now on.

Table 3.4 Review of the interface dimension depending on the mesh

	<i>Old geometry</i>	<i>New geometry</i>	
<i>Number of cells</i>	56 731	55 798	119 651
<i>Interface dimension [μm]</i>	17.7	27.4	13.6

Until now and as mentioned before, the simulations performed have had the time step set to $10 \mu\text{s}$ and, as it is a quite large one, it was decided to lower it by setting it to half the value that was being used, precisely $5 \mu\text{s}$. This time step had been already tested and used in a previous similar study made by Carlos Moreno [32], and it was used for this reason.

3.2.2 Boundary conditions evaluation

After all that, the thick part of the simulations starts by searching for the ideal boundary conditions for a determined velocity, which was $6 \mu\text{l}/\text{min}$ for both fluids and for a specific amount of time, which was 0.0512 seconds.

During these simulations, the boundary conditions were changed following a pattern and symmetry conditions, for instance, walls 1 and 2, 4 and 5, 6 and 7, 10 and 11 and 12 and 13 (see Fig. 2.7), each pair used the same boundary condition. As expected, the first boundary conditions that were tried were the ones chosen for the other geometry, however, they did not perform good results on this one. The droplets were formed, however the first one coalesced with the second one, the third with the fourth and so on. For this reason, it was thought that the search for these conditions had to be started from the beginning again.

To start up with, the values for walls3 always remained in 0 because the dispersed phase did not arrive to make contact with this wall. Additionally, walls12 and walls13 also remained with the 0 value, considering that the droplet did not have to touch these walls.

Walls8, walls9, walls10 and walls11 started having values between 5 and 15, but eventually they switched to 0 because it gave better results. It was believed that the critical walls were walls6 and 7 because they were the neck ones, therefore these were the ones that experienced most of the variations. Walls1, walls2, walls4 and walls5 experienced also a lot of changes, however the values were close to 65.

These tests were done by trial and error. Some contact angles were changed and depending on the results obtained, the contact angles were changed up and down in order to see how they evolved, but also to compare them with the previous ones.

In this part, 42 simulations were performed, taking about 160 hours to run in total. All the contact angles used for this trial can be seen in Appendix C.2.1. While performing them, it could be noticed that the bigger the contact angle at walls6 and 7, the more probable would be that the droplet could not form completely, because it remained attached to one of these walls and did not break. Therefore, the tendency that was followed was to decrease the angles. However, the right combination of contact angles at the rest of the walls had not been achieved yet, and for this reason, they were changed several times as well. Despite all this, the minimum relative error made among all these first simulations is of 4.8% for the diameter and 11% for the normalized volume.

When performing these first 42 simulations an unexpected problem was encountered; the droplets were generated normally but they were absorbed by the outlet, and they did not flow properly through it. This could have been caused by the mesh not being enough dense there, or not having the correct boundary conditions at the outlet.

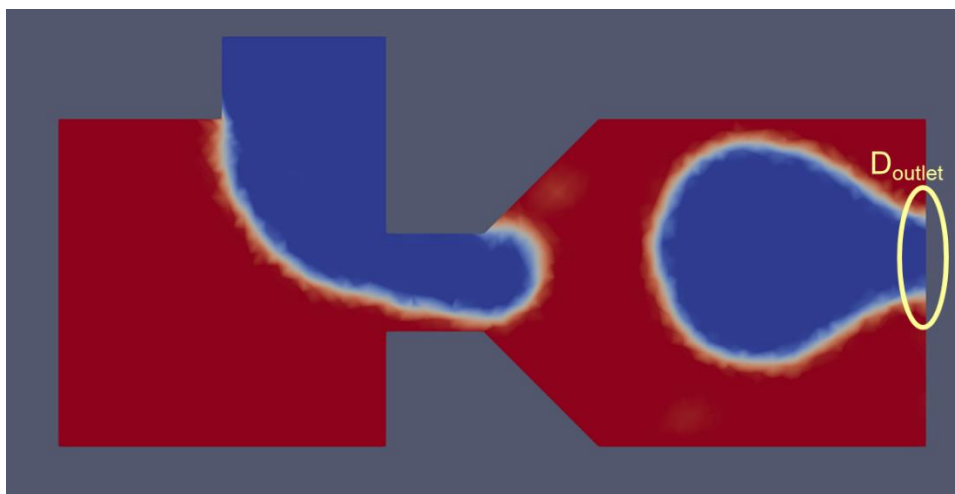


Fig. 3.11 Example of suction of the droplets at the outlet

For this reason, to start up, it is decided to set new boundary conditions for the outlet in order to test them. 12 more simulations were performed, just changing the boundary conditions on the outlet, while the contact angles remained the same as in the last simulation done. The problem could not be solved, even though all the common and most usual boundary conditions were tested [30].

Fig. 3.12 shows the diameter of the droplet achieved in the simulation versus the diameter of the droplet when it is exiting the capillary, which is when it is being sucked out from it. The x-axis represents the number of simulation, being the first one the one that was being used until now and the rest are the new boundary conditions tried at the outlet, whereas the y-axis shows the diameter of the droplet. In light green the diameter of the droplet at the capillary can be seen and in dark green the diameter at the outlet is shown (see Fig. 3.11).

If there was no problem with the boundary conditions at the outlet, droplets would exit the capillary having the same size as they did before, and for this reason, plot shown in Fig. 3.12 presents this difference. Therefore, the desired solution would be having both lines in the plot being as close as possible.

As can be appreciated, the new boundary conditions tried were worse than the one that was already being used, for this reason, the same boundary conditions as presented in table 3.1, table 3.2 and table 3.3 for the outlet were used. It has to be noticed that despite trying 12 boundary conditions, only 3 new ones formed droplets and for this reason there are only 4 values in the plot. In order to see the different boundary conditions tried, see Appendix C.1.

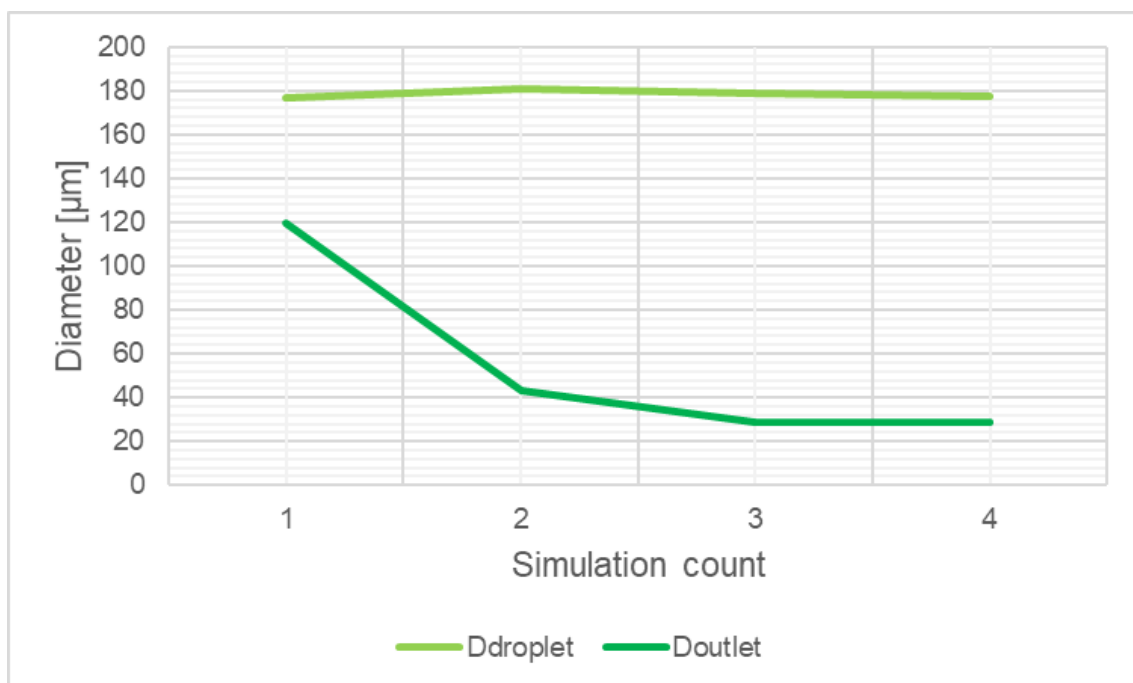


Fig. 3.12 Droplet diameter at the outlet

As the problem regarding the outlet's boundary conditions had not been solved, it was time to start thinking about performing the second option which was redoing the mesh, but much denser. For this reason, it was thought that creating two more meshes to compare them to the one already done would be interesting. And so it was, two meshes were made, one with double the cells and the other with half of them, as can be seen in the Fig. 3.13.

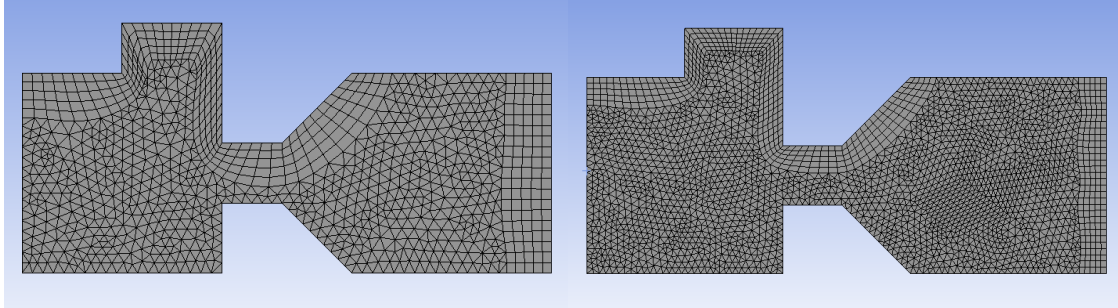


Fig. 3.13 Comparison between the mesh with half the cells (A) and the one with the double (B).

The characteristics of these new meshes were the same as in the old ones, in order to be able to compare them better. However, there is one crucial modification; at the outlet, the cells of the mesh were tighter so that it was easier to see if there was any notorious change.

This modification was done just by adding one more wall to the inflation characteristic, the outlet one. Mesh A has a total of 62 106 cells, whereas B has 259 853. As mentioned before, in order to change the number of cells, the size of the elements must increase or decrease, depending on the desired mesh; for mesh A, the size was $1.02 \cdot 10^{-5}m$ while for B, it was $6.5 \cdot 10^{-6}m$.

The following table (table 3.5) shows a review of the dimension of the droplet at the outlet, while it is being sucked out of the geometry. As it can be seen, between the previous mesh and mesh B, there is a small decrease in this dimension. However, there is a large increase in the simulation time, for this reason the mesh that it is going to be used for the following simulations is the “previous mesh” from table 3.5 which corresponds to Fig. 3.9.

Table 3.5 Review of the droplet dimension depending on the mesh

	<i>Mesh A</i>	<i>Previous mesh</i>	<i>Mesh B</i>
<i>Number of cells</i>	62 106	119 651	259 853
<i>Droplet dimension outlet [μm]</i>	17.4	11.9	10.6
<i>Simulation time [s]</i>	10 385	21 980	72 621

Despite trying the two options mentioned above for the boundary conditions on the outlet, the problem could not be solved and the droplets still left the capillary as if they were being sucked out. This obstacle remained there and could not be overcome for now, but was always kept in mind in case a new solution occurred.

Given that following the outlet matter there was no way to continue, the seek for the ideal boundary conditions persisted. Therefore, following the same patterns explained before about how the angles changed for every simulation, 34 more were performed taking approximately 100 hours to run in total.

Eventually, some limiting but acceptable conditions were found, having just a 0.24% of relative error in the diameter measure and a 0.5% in the volume one. It was difficult finding these conditions because in some cases if the values of the walls were lowered the first droplet would combine with the second one, creating a much bigger droplet than desired. However, if the boundary conditions increased, the droplet did not form completely because it did not break and it also got stuck after the “breakup” stage.

3.2.3 Validation of the solution

The conditions that were chosen to be the best ones among all the ones already performed were the ones that had walls 1, 2, 4 and 5 set to 65 degrees (180-65 real degrees), wall 6 to 85 degrees, wall 7 to 110 degrees and the rest set to 0 degrees.

In Fig. 3.14 the evolution of the droplet formation can be appreciated, as well as the different stages it has. The comparison between the experimental and the simulation can also be appreciated.

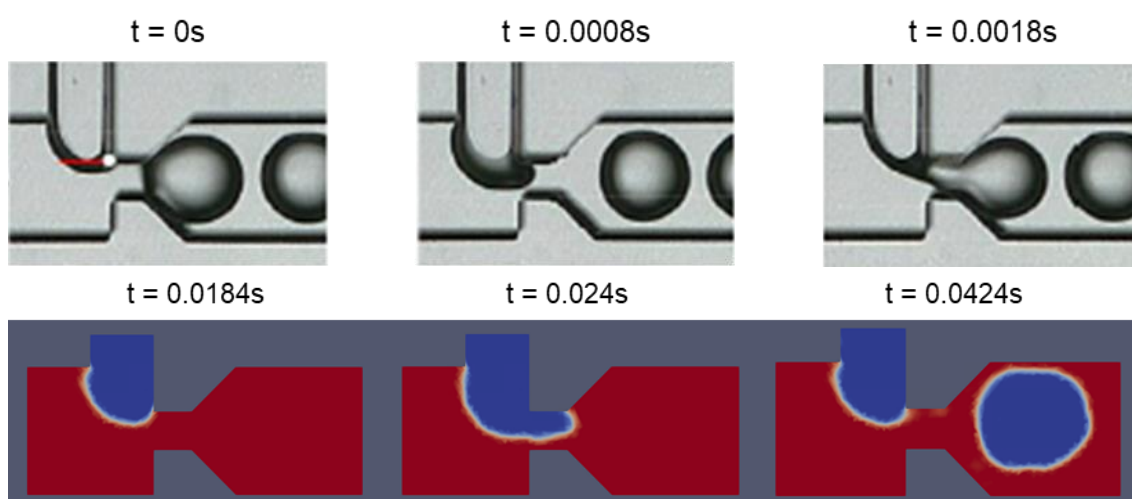


Fig. 3.14 Evolution of the droplet formation for the boundary conditions chosen.

This simulation was not ideal and did not follow the paper's droplet formation stages nor timings, because, as explained in the previous subchapter, the simulation time until a droplet was formed should be of 0.018s and here it takes 0.024s. However, comparing the diameter and volume parameters, it seemed good enough. Additionally, when the droplet was at the neck, it should touch both walls⁶ and 7 and it did not do that.

In spite of all this, as the geometry was going to be changed again and, between the first and the second one the boundary conditions chosen were not useful, it was thought that a closer solution would be enough; so that the amount of simulations for the last geometry, the longer ones, would be decreased.

These conditions were the ones selected to be used in the following geometry which will be explained in the next and last part of the evolution of the simulations, the final data gathering.

3.3 Final data gathering

The final step remaining for this project was to try the chosen boundary conditions and perform several simulations to get the wanted data, in order to make the graphics comparing the volume and the diameter. The plan was to compare these parameters with the real geometry and the one used in the previous chapter, with different velocities and different meshes, but with the same boundary conditions.

In Fig. 3.1 previously shown in Chapter 3.1, the third and real geometry can be seen with its dimensions. For this geometry, a new mesh was created as a base to start up, with approximately the same amount of cells as the largest mesh for the last geometry, specifically this one has 267 213 cells. This was done because as it was a bigger geometry, it would need more cells, as seen in the previous subchapter (see Fig. 3.15).

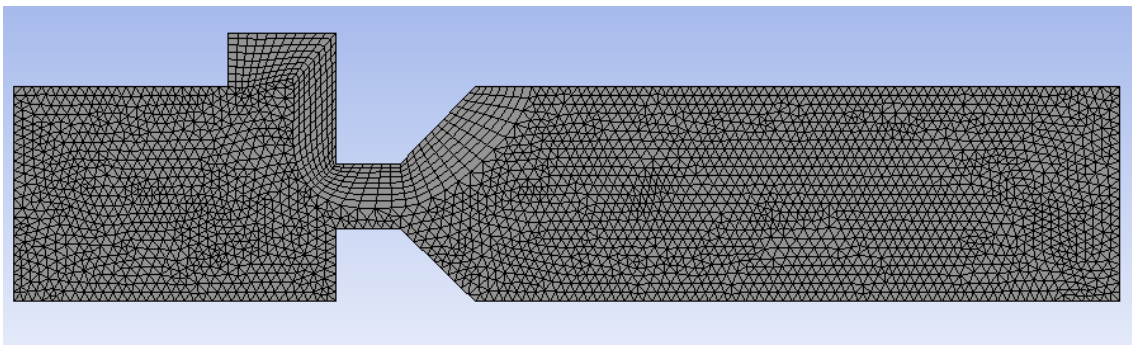


Fig. 3.15 New mesh for the complete geometry

- Type of mesh: CFD compatible, fluent, linear with a tetrahedral method and patch-conforming algorithm.
- Body sizing: the element size is $8.6 \cdot 10^{-6}$ m.
- Inflation: 8 layers with a growth rate of 1.2 and a maximum thickness of $1 \cdot 10^{-4}$ m.

The main idea was to plot different graphics using different meshes to be able to compare them and see if there was an improvement or not between them, just like had been done with the previous mesh. Therefore, two extra meshes were created, one with half the cells and the other with the double.

The characteristics of these new meshes were mainly the same as in the ones shown in Fig. 3.15, in order to be able to compare them better. The mesh with half the cells has a total of 140 250 cells, whereas the denser one has 530 851. As mentioned before, in order to change the number of cells, the size of the elements must increase or decrease, depending on the desired mesh. For the lighter one, the size was $1.05 \cdot 10^{-5}$, while for the denser one it was $6.7 \cdot 10^{-6}$. Table 3.6 has a summary of all the meshes that were going to be used.

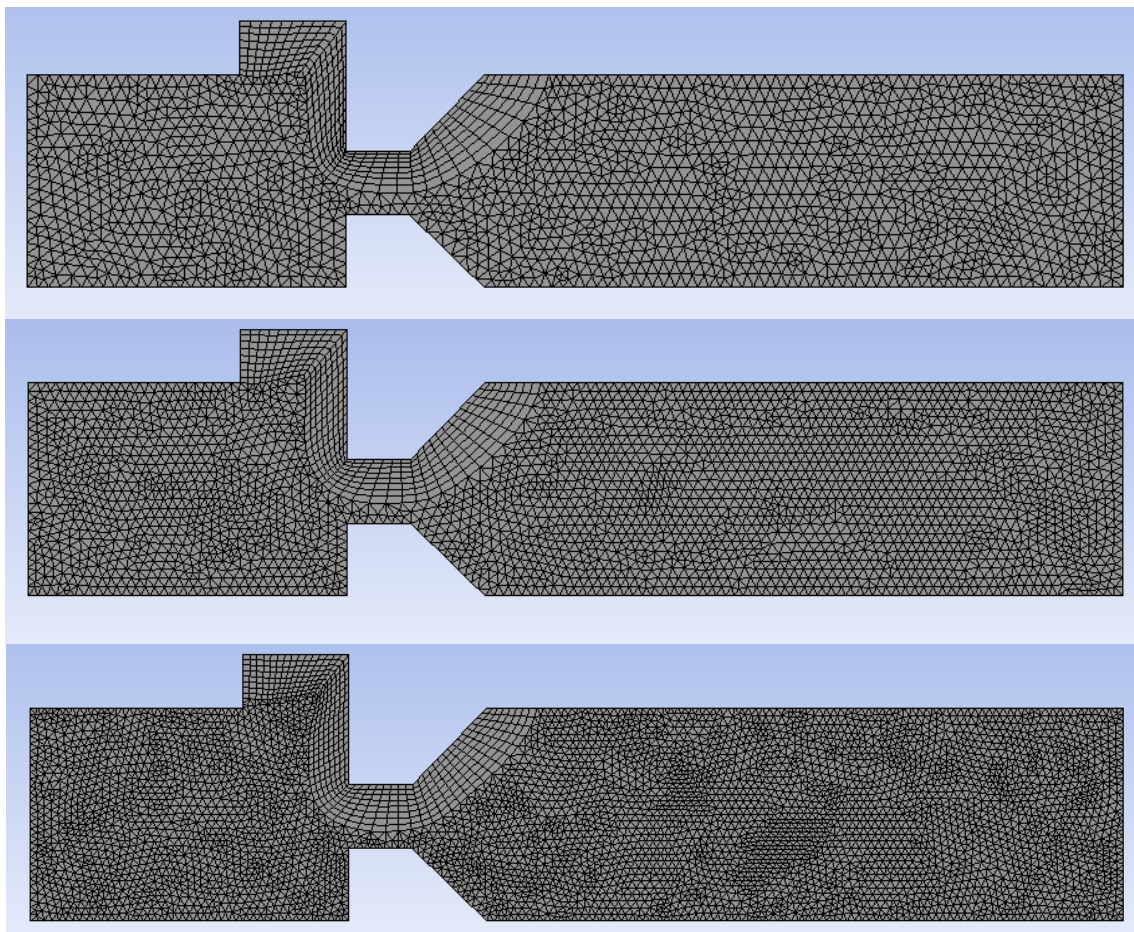


Fig. 3.16 The three meshes used; the top one ($n/2$), the middle one (n) and the bottom one ($nx2$)

The amount of layers changed as well, because it was thought that for the final data gathering it was important to have more accuracy in these critical parts, but without making it as in the first mesh for the first geometry. In Fig. 3.16 these new meshes with respect to the old one can be seen.

In order to do the simulations for the second geometry, the old meshes that were previously used to check the boundary conditions at the outlet, were reutilised and they can be seen in Fig. 3.10. In table 3.6 a summary of the meshes that were going to be used can be seen, with the parameters that did change between each of them.

Some of the parameters did not change, like the type of mesh and the growth rate and maximum thickness of the inflation. The number of cells will be represented with the letter “n” and it will be used to indicate if the mesh is denser “nx2” or if it has less cells “n/2”.

Table 3.6 Summary of the different characteristics of each mesh

	<i>Second geometry</i>			<i>Third geometry</i>		
	n/2	n	nx2	n/2	n	nx2
<i>Nº cells (n)</i>	62 106	119 651	259 853	140 250	267 213	530 851
<i>Cell's size</i>	$1.02 \cdot 10^{-5}$	$8.5 \cdot 10^{-6}$	$6.5 \cdot 10^{-6}$	$1.05 \cdot 10^{-5}$	$8.6 \cdot 10^{-6}$	$6.7 \cdot 10^{-6}$
<i>Inflation's layers</i>		5			8	

As mentioned before, the velocity of the fluids was one of the parameters that was chosen to change throughout the simulations, using some of the ones showed in the paper. With all of that done, it was time to decide the simulation time, which would be 0.3 seconds for all the simulations, and to start sending them to the cluster, following the steps shown in Appendix A.2.

The simulations for the second geometry were performed using the boundary conditions chosen in the Chapter 3.2 and with different velocities. Looking at the results it could be checked that these boundary conditions did not work for all the velocities, because for some of them the droplet was way bigger and for some others it did not even form completely.

In spite all this, the third geometry was tested as well, performing the same type of simulations as for the second one. The results were worse and unusable, just as before, the boundary conditions from the second geometry did not work for the third one; they only worked to have a clue to continue searching and not start from the beginning.

For these reason the plan had to be changed. Since there was not enough time to start again and look for new boundary conditions for both geometries, it was decided to do just the third one, because it was the one used in the paper. So different geometries were not going to be compared, nor different meshes. However, the velocities were going to be changed as can be seen in table 4.1 and table 4.2 of the following chapter.

And again, new simulations with the mesh shown in Fig. 3.15 and with a velocity of $Q_C = 8 \mu l/min$ and $Q_D = 4 \mu l/min$ were performed to try to find the most accurate boundary conditions. They were started to get changed following the same pattern as they did for the old geometry, but just changing walls6 and 7 which were the most critical ones. The simulation time was decided to change as well, and make it lower, because some of the simulations performed before took almost a week to complete, which was too much time. Therefore, it was settled to 0.1s.

After that, when they were found for this specific velocity, the boundary conditions for walls1 and 2 were checked, because theoretically, there should be a thin layer of oil between the droplet and the wall, and there was not (see Fig. 3.17). Therefore, some more simulations were performed checking just that and leaving all the other walls as they were. As can be checked in the figure, the best is the first one, which performs a more defined droplet.

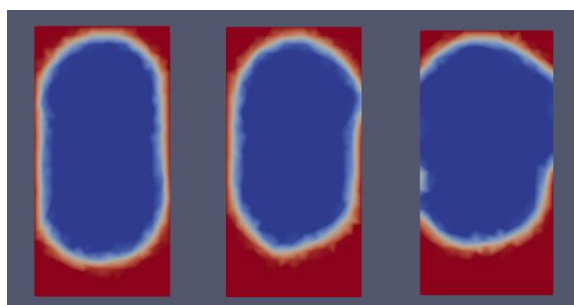


Fig. 3.17 Close-up look at walls1 and 2 at 0° , 15° and 30° , respectively

Following that, the other velocities started to be tried with the boundary conditions found, however, as expected, they did not work correctly and they had to be changed as well in order to adapt the results and make them more accurate. This was done by trial and error, as they did not have to change quite much, just some degrees up or down. Nevertheless, each definitive simulation took 2.5 days to complete, therefore, this part of the study took more than a month to complete.

During these final simulations using the third geometry, another inconvenient appeared. The droplets were not form right away, first a small droplet was formed, getting stuck after the neck and not moving forward through the channel. Then a second droplet was formed, which coalesced with the first one to, later on, start flowing all the way to the outlet. This problem had also came out during some of the simulations of the last geometry, however it did not always happen.

This could have been caused because as there was such a little time for the simulations (0.0512s), the problem did not appear, but it had always been there and now that the simulations took more time (0.1s) the problem was more noticeable. In spite all of this, several boundary conditions were tried but none of them gave the results straight away. If the contact angle was bigger, the droplet did as well, and if they were smaller, the same problem occurred.

Eventually, the only step left that remained was to gather all the data and plot the final results which can be found in the following chapter (Chapter 4). The final list with all the definitive contact angles can be found in Appendix C.2.2, as well as the different files utilized, can be found in Appendix A.1.

CHAPTER 4. RESULTS

In this part of the project, an in-depth analysis of the obtained results for the definitive simulations will be done. Different graphics will be shown, representing mainly the diameter and the volume, as well as a comparison with the results that were obtained in the scientific paper [1].

Some other plots have been done during the study. In Chapter 3.2, there is Fig.3.12 showing how the outlet boundary conditions affected the droplet diameter there. Different tables have been done as well, showing comparison results between meshes (see Table 3.5 and Table 3.6) and comparing the dimensions between the interface of both fluids with different meshes as well (see Table 3.4). Finally, in Appendix C.2.1, two more plots regarding the evolutions of the experiments toward the desired goal can be seen.

Before showing any results, it is important to recall some critical parameters that were used to perform these simulations. The final T-junction geometry with the 267 213 cells mesh can be seen in Fig. 3.15. Eventually, the simulation time was set to 0.1s with a time step of 5 μ s.

The main idea was to do a total of 8 simulations, each of them having a different velocity, but with the same boundary conditions. Unfortunately, this was not possible because the same contact angles did not work for each velocity. For these reason they were decided to change so that the results were more accurate and resembled the paper.

The table with all the contact angles used for each wall can be seen in Appendix C.2.2 and all the data is gathered in Appendix B. In Appendix A.3 the different tools used to do all the measurements can be checked, as well as a brief tutorial on how to do it.

The chosen velocities can be seen in Table 4.1 and Table 4.2 , as well as the flow rate ratio (α) and the capillary number for the continuous phase (Ca_c).

Table 4.1 Velocities and Capillary numbers for $\alpha = 1$

$Q_c = Q_d$		U_c	U_d	Ca_c
$[\mu\text{l}/\text{min}]$	$[\text{m}^3/\text{s}]$	$[\text{m}/\text{s}]$	$[\text{m}/\text{s}]$	
8	$1.33 \cdot 10^{-10}$	0.0067	0.0133	0.0105
6	$1 \cdot 10^{-10}$	0.005	0.01	0.0078
4	$6.67 \cdot 10^{-11}$	0.0033	0.0067	0.0052
2	$3.33 \cdot 10^{-11}$	0.0017	0.0033	0.0026

Table 4.2 Velocities and Capillary numbers for $\alpha = 0.5$

Q_c		Q_d		$U_c = U_d$	Ca_c
$[\mu\text{l}/\text{min}]$	$[\text{m}^3/\text{s}]$	$[\mu\text{l}/\text{min}]$	$[\text{m}^3/\text{s}]$	$[\text{m}/\text{s}]$	
8	$1.33 \cdot 10^{-10}$	4	$6.67 \cdot 10^{-11}$	0.0067	0.0105
6	$1 \cdot 10^{-10}$	3	$5 \cdot 10^{-11}$	0.005	0.0078
4	$6.67 \cdot 10^{-11}$	2	$3.33 \cdot 10^{-11}$	0.0033	0.0052
2	$3.33 \cdot 10^{-11}$	1	$1.67 \cdot 10^{-11}$	0.0017	0.0026

4.1 Analysis of the droplet diameter

In this part of the results, a wider study of the droplet diameter will be done, where Ca_c and α are chosen to document the size of the droplets formed.

The diameter was calculated with the tool “ruler” in ParaView (see Appendix A.3). There the horizontal and vertical measurements of the droplet were done and the average value between them, calculated (see Appendix B). This was going to be the value used in the plots. However, the simulations showed more than one droplet, two or three depending on the simulation, for this reason the best value between them was chosen, which was the one of the last droplet generated.

In Fig. 4.1 a comparison between the experimental and the simulation diameter results is shown, for different capillary number (Ca_c) and different flow rates (α), as mentioned before. The exact plot with the experimental data can be seen in Fig. 2.2, from where the data was extracted. In dark and light pink, the experimental results can be seen with its tendency lines, whereas the simulated ones can be seen in green. For the flow rate ratios $\alpha = 1$ the results are represented on the plot with a square and for $\alpha = 0.5$, they are shown with a dot. So the green squares should be close to the pink squares and the same for the dots.

It can be seen that the diameter is significantly reduced when the Ca_c increases. In addition, for the cases where $\alpha = 1$, the droplet is bigger, whereas for $\alpha = 0.5$ is smaller. Thus, it can be said that the droplet size increases with α , but it decreases with the Capillary number. Considering that the Capillary number depends on the velocity (see Eq 2.7), an increase in the velocity would mean an increase in the Ca_c and, consequently a decrease in the diameter.

So, the bigger the velocity of the continuous phase with respect to the dispersed one, the smaller the droplet will be. Since the pressure at the neck will be bigger, the droplet will break faster. This phenomenon would explain the relation between the diameter and the Ca_c , α and velocity.

Table 4.4 shows all the data gathered for this subchapter's plots, presenting the diameters for each flow rate ratio, the Capillary numbers and both the absolute and relative errors produced during the simulations.

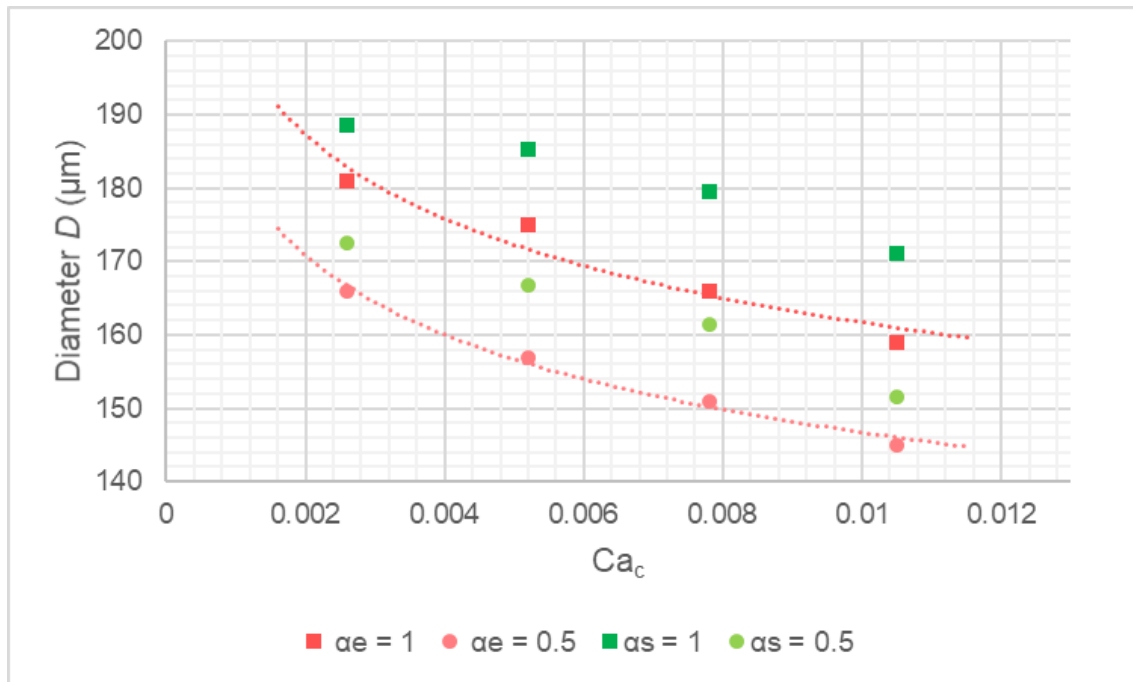


Fig. 4.1 Comparison between experimental and simulated data of the dependence of droplet diameter on Ca_c under the same α

Even though in Fig 4.1 all the points differ from tendency lines and seem to have very different values from the ones of the experiments, the variation stands between 4-9%, as can be seen in table 4.4. Also, the average difference between the experimental and simulated values stands at $10.9 \mu\text{m}$ for $\alpha = 1$ and of $8.6 \mu\text{m}$ for $\alpha = 0.5$. It can also be noticed that all the values obtained at the simulations are bigger than the experimental ones.

With this deviation, it is possible to say that the results are not really accurate and could be improved. Not forgetting that, the simulations generated double the amount of droplets and the measurements were done on the one generated by the coalescence between the first and the second, which was the one that stabilized its shape at the end of the capillary.

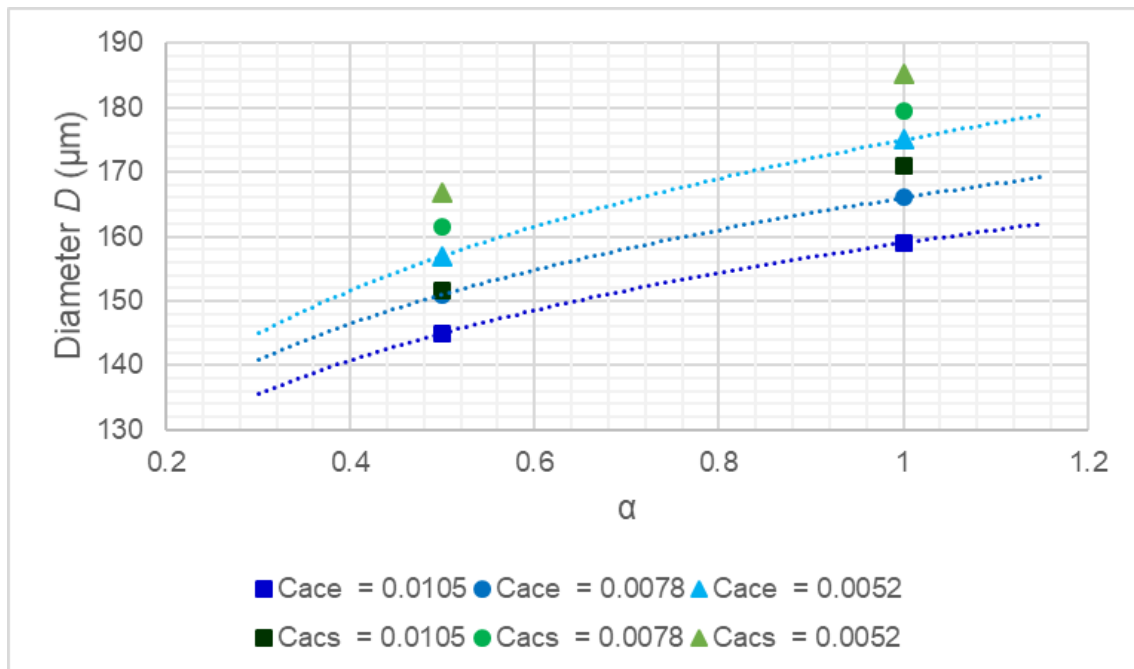
However, as mentioned at the beginning of this subchapter, there was more than one droplet produced per simulation. The more droplets produced, the less error it had. For this reason, it would be interesting to keep in mind that this error could be decreased just by performing longer simulations. These results can be checked at Appendix B. However, Table 4.3 shows a small part of it showing how the relative error decreases.

Table 4.3 Improvement of the relative error for simulation $Q_c = Q_d = 8 \mu\text{l}/\text{min}$

Droplet	$D [\mu\text{m}]$	$e_{ad} [\mu\text{m}]$	$e_{rd} [\%]$	V_n	e_{av}	$e_{rv} [\%]$
1	207.0	48.5	30.6	0.69	0.33	91.9
2	188.8	30.3	19.1	0.56	0.2	56.5
3	171.0	12.5	7.9	0.45	0.09	25.5

Table 4.4 Experimental vs. Simulation data for the diameter with the error

		Experiment		Simulation					
		$\alpha=1$	$\alpha=0.5$	$\alpha=1$	$\alpha=0.5$	$\alpha=1$		$\alpha=0.5$	
Q_c	Ca_c	$D [\mu\text{m}]$		$D [\mu\text{m}]$		$e_a [\mu\text{m}]$	$e_r [\%]$	$e_a [\mu\text{m}]$	$e_r [\%]$
8	0.00105	158.5	144.5	171	151.5	12	7.87	7	4.83
6	0.0078	165.5	150.5	179.5	161.4	14	8.43	11	7.24
4	0.0052	175	157	185.2	166.8	10	5.84	9.8	6.21
2	0.0026	181	166	188.6	172.5	7.6	4.2	6.5	3.92

**Fig. 4.2** Comparison between experimental and simulated data of the dependence of droplet diameter on α under the same Ca_c

In Fig. 4.2 the variation of the diameter with respect to the flow rate ratio under the same Ca_c is represented. This time the experimental values and tendency lines are shown in blue and, as for the previous one, the simulated is in green. It can be noticed that the values for $Ca_c = 0.0026$ are not expressed, this is because in Fig. 2.3, the plot which is trying to be reproduced, they are not shown.

Just as for the last plot, the same predisposition can be seen. Diameter increases when α increases and it decreases when the capillary number increases. When the capillary number is low, the dispersed phase fluid tends to occupy the full width of the main channel, whereas when the capillary number increases the dispersed phase fluid occupies only part of the main channel, and smaller droplets are formed. Therefore, when the neck is completely obstructed by the dispersed phase, the pressure increases significantly, breaking the droplet. If $\alpha=1$, the dispersed phase has a bigger velocity than the continuous phase. So, the continuous phase will need more time to increase the pressure and break the droplet. During this time, more dispersed phase will have passed the neck, making the droplet bigger.

4.2 Analysis of the droplet volume

Another important parameter to analyse and compare is the volume, which can be calculated following Eq. 4.1 for a single-direction confined droplet shown in the paper. Although there, the dimensionless volume (V_n) is considered for all the plots. For this reason, it is essential to know how to calculate it, which is following Eq. 4.2.

$$V = \pi h \cdot \left(\frac{D-h}{2}\right)^2 + \frac{(\pi \cdot h)^2}{4} \cdot \left(\frac{D-h}{2} + \frac{2h}{3\pi}\right) \quad (4.1)$$

$$V_n = \frac{V}{h \cdot w_c^2} \quad (4.2)$$

Where V is the volume of the droplet, h is the depth of the capillary, D is the diameter of the specific droplet and w_c is its width.

Now that these parameters are introduced, it is time to calculate them to, later on, make the different plots. Just as for the diameter, there are two key ways of plotting this data: normalized volume vs. Ca_c (see Fig. 4.3) and normalized volume vs. α (see Fig. 4.4). These two graphics with the simulated data can be appreciated in Fig. 2.3. It has to be noticed that the experimental value of the volume for the $\alpha = 0.5$ and $Ca_c = 0.0026$ could not be plotted as it was not shown in Fig. 2.3.

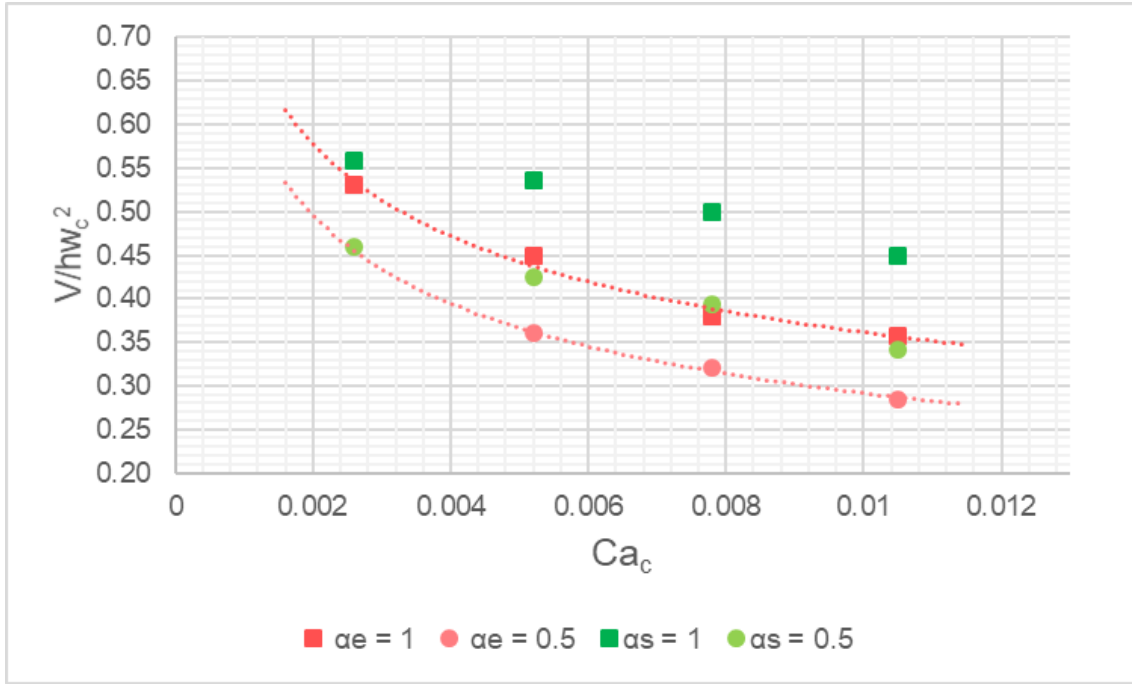


Fig. 4.3 Comparison between experimental and simulated data of the dependence of the normalized droplet volume on Ca_c under the same α

In Fig 4.3 the comparison plot between experimental and simulated data of the dependence of the normalized droplet volume on Ca_c under the same α can be seen. The colour combination is the same as the one explained in Fig. 4.1.

Looking at this plot, it is possible to see that the volume considerably decreases with the increase of the Ca_c and that by reducing α there is a significant drop in the droplet volume, as well. These ideas are in complete agreement with the ones explained for Fig. 4.1 and Fig. 4.2.

The fitted curved shown in Fig. 4.3 was created using Eq. 4.3, which would be equation 9 from the paper, where ζ is a fitted coefficient varied with α . In the paper for this exact plot, there was no data for $\alpha = 0.5$, which is one of its main values in the simulations, however, it was possible to calculate them using Eq. 4.4 and validate them by checking the plot from Fig. 2.3 (b).

$$\frac{V}{h \cdot w_c^2} = \zeta Ca_c^{-0.3} \quad (4.3)$$

$$\frac{V}{h \cdot w_c^2} = a + b\alpha^{0.5} \quad (4.4)$$

In Fig. 4.4 the variation of the volume with respect to the flow rate ratio under the same Ca_c is represented. Just as for the Fig. 4.2, colour blue shows the experimental results and the green ones, the simulation ones.

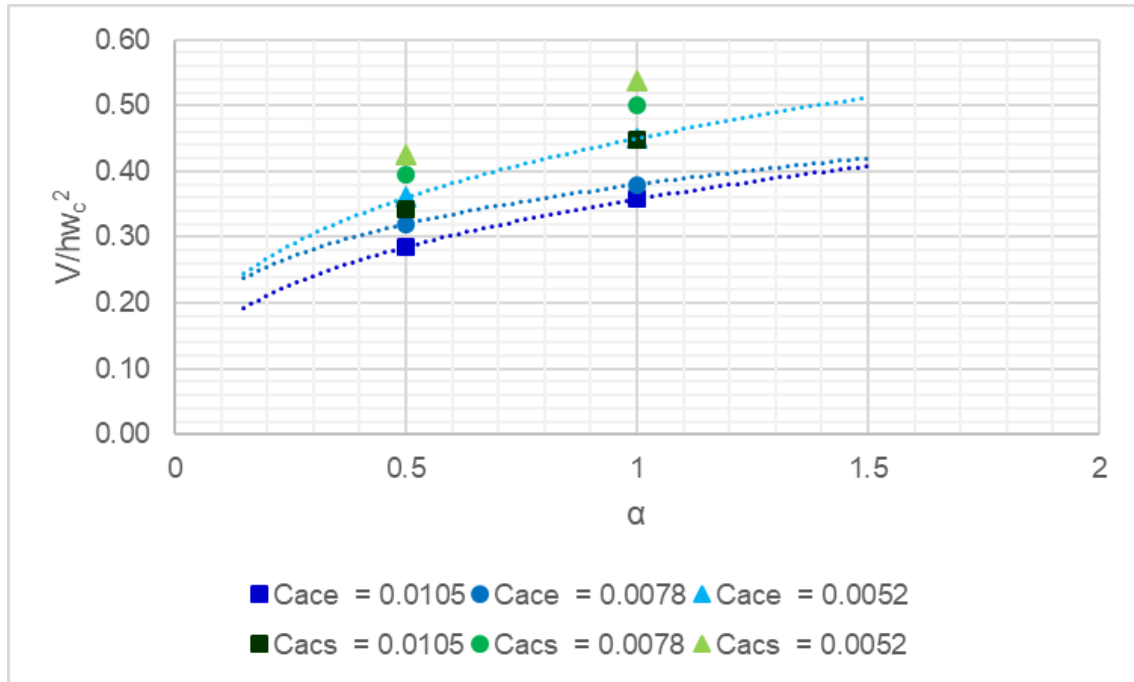


Fig. 4.4 Comparison between experimental and simulated data of the dependence of the normalized droplet volume on α under the same Ca_c

Finally, in table 4.5 the results for the analysis of the droplet volume can be seen, as well as the different error produced during the simulations. As seen in Fig. 4.3 the volume seems to differ substantially between the experimental and the simulations and table 4.5 shows that indeed, they do. The relative error between them is around the 20% for most of the cases, which is major error for the validation of the results. This can be explained looking at Eq. 4.1, where there is the diameter squared and also, the diameter multiplying a big nominator, meaning that a small error on this parameter would increase the volume error significantly. This seems to have happened here, increasing the error made in the simulations.

Table 4.5 Experimental vs. Simulation data for the volume with the error.

		<i>Experiment</i>		<i>Simulation</i>					
		$\alpha = 1$	$\alpha = 0.5$	$\alpha = 1$	$\alpha = 0.5$	$\alpha = 1$	$\alpha = 0.5$		
Q_c	Ca_c	V_n	V_n	V_n	V_n	e_a	e_r [%]	e_a	e_r [%]
8	0.00105	0.36	0.29	0.45	0.34	0.09	25.51	0.06	19.89
6	0.0078	0.42	0.32	0.50	0.39	0.08	19.02	0.07	23.33
4	0.0052	0.45	0.36	0.54	0.42	0.09	19.19	0.06	17.85
2	0.0026	0.53	0.4	0.56		0.03	5.34		

To sum up all the results shown in this chapter, it is possible to say that with the increase of the Capillary number, the droplet volume decreases and with the decrease of the flow rate ratio, the volume also drops. However, this is exactly the same that happened with the diameter. Therefore, as expected, both the diameter and the volume are correlated, meaning that, the larger the Capillary number and the flow rate ratio, the larger will be the volume and by extension the diameter of the droplet.

If this last statement is analysed, it makes total sense, because if the Ca_c increases, this will mean that the velocity of the continuous phase increases (Q_c) as well. So, if the Q_c increases, α will decrease and the volume and the diameter will be smaller. This phenomenon could be explained thinking that when the droplet is forming, if the Q_c is bigger, it will make more pressure on the droplet, making it break earlier than if the velocity of both fluids was the same. However, pressure is not the only force promoting the droplet formation. Surface tension existing at the liquid-liquid interface and the viscous force exerted by the continuous phase strongly contribute to the discontinuous phase breakup.

CHAPTER 5. CONCLUSIONS

This project has presented a study of the droplet generation under different flow rates in a T-junction with a neck using numerical simulations with OpenFOAM with the later post-processing of the data using ParaView and Excel. It is based on the article "Droplet generation under different flow rates in T-junction microchannel with a neck" [1].

One of the main things that were checked before the start of the experiments was the dimensionless numbers that verified the type of experiment that was being performed. It was determined that the Capillary number would take an important role in the experiment and that the main forces that would drive the droplet formation would be the capillary ones.

After the creation of the geometry, the definition of the different boundaries and the mesh creation; the most important part of the project and, by far, the most difficult one, was the seek for the boundary conditions at the wall that made the droplets generate as in the article. Therefore, several simulations were performed until the finding of the perfect fit for a specific velocity, which was $Q_c = 8 \mu l/min$ and $Q_d = 4 \mu l/min$. As it was decided to perform the simulations with 4 different velocities for the continuous phase, but with different flow rates ratios, new boundary conditions had to be found for the remaining cases.

Eventually, the boundary conditions for all velocities were found and the only remaining task left was to plot the collected data into different graphics in order to analyse the chosen parameters which were the droplet diameter and volume. Both of them were plotted under the same capillary number or the same flow rate ratio, which stated that the larger the Capillary number and the flow rate ratio, the larger would be the volume and, by extension, the diameter of the droplet. Additionally, a comparison with the results of the experiments shown in the paper was done in order to check the error made during the simulations. Finally, it was determined that the error was considerably significant and, for this reason, the simulations were not completely successful.

This study could be continued and improved in several ways. Further research is needed to determine the causes of the boundary conditions at the outlet that make the droplets exit the capillary as they were being sucked out it. Moreover, more accurate boundary conditions could be found for each and every velocity used to have less error and, most importantly, to create directly one droplet, not two that merge together. Additionally, in the paper the scientists mention that the flow is left for 20 minutes before recording any images of the droplets. This could be tried, just for the purpose of checking if the error gets better or if the droplets form correctly. Finally, using the equation created in the paper to calculate the volume of a droplet, a volume for a specific velocity could be calculated to, later on, perform some simulations and verify that the results match.

BIBLIOGRAPHY

- [1] Yan Pang, Qiang Zhou, Xiang Wang, Yanghao Lei, Yanlin Ren, Mengqi Li, Ju Wang and Zhaomiao Liu, "Droplets generation under different flow rates in T-junction microchannel with a neck", *AIChE Journal*, (2020).
- [2] Arias S. and Montlaur A., "Influence of Contact Angle Boundary Condition on CFD Simulation of T-Junction", *Microgravity-Science and Technology*, pp.1-9 (2018).
- [3] Microgravity and ISS – ESA
https://www.esa.int/Education/Orbit_Your_Thesis/Microgravity_and_ISS2
On-line
- [4] What is Microgravity – NASA
<https://www.nasa.gov/centers/glenn/shuttlestation/station/microgex.html>
On-line (2009)
- [5] Why Do Science in Microgravity? – NASA
https://www.nasa.gov/mission_pages/station/research/station-science-101/why-do-science-in-microgravity/ On-line
- [6] Funmilola A. Oluwafemi and Adhithiyan Neduncheran, "Analog and simulated microgravity platforms for life sciences research: Their individual capacities, benefits and limitations", *Elsevier* (2022).
- [7] Francesca Ferranti, Marta Del Bianco and Claudia Pacelli, "Advantages and Limitations of Current Microgravity Platforms for Space Biology Research", *MDPI* (2020).
- [8] Trisha Muro and Bethany Brookshire, "Explainer: Gravity and microgravity", *ScienceNewExplores*, (2022).
<https://www.snexplores.org/article/explainer-gravity-and-microgravity>
- [9] James E. Faller, "gravity", *Britanica*, (2022).
<https://www.britannica.com/science/gravity-physics>
- [10] Job Nijhuis, Svenja Schmidt, Nam Nghiep Tran and Volker Hessel, "Microfluidics and Macrofluidics in Space: ISS-Proven Fluidic Transport and Handling Concepts", *Frontiers Space Technologies*, (2022).
- [11] Sruthi Jagannathan, "Microfluidics for Liquid Biopsies", *Mechanobiology Institute*, National University of Singapore, (2016)
- [12] Dan Liu, Meilin Sun, Jinwei Zhang, Rui Hu, Wenzhu Fu, Tingting Xuanyuan and Wenming Liu, "Single-cell droplet microfluidics for biomedical applications", *Departments of Biomedical Engineering and Pathology, School of Basic Medical Science, Central South University, Changsha, Hunan*, (2022)

- [13] Sanjiv Sharma, Monpichar Srisa-Art, Steven Scott, Amit Asthana and Anthony Cass, "Droplet-Based Microfluidics", Humana Press, (2012).
- [14] What is microfluidics – News Medical Life Science
<https://www.news-medical.net/life-sciences/What-is-Microfluidics.aspx>
- [15] Sunflower oil - Wikipedia
https://en.wikipedia.org/wiki/Sunflower_oil
- [16] Properties of water - Wikipedia
https://en.wikipedia.org/wiki/Properties_of_water
- [17] Dimensionless numbers and their importance in fluid mechanics - *The constructor*
<https://theconstructor.org/fluid-mechanics/dimensionless-numbers-importance-fluid-mechanics/34265/>
- [18] Reynolds number- The Engineering ToolBox
https://www.engineeringtoolbox.com/reynolds-number-d_237.html
- [19] Fluid Flow - Hydraulic Diameter, - The Engineering ToolBox
https://www.engineeringtoolbox.com/hydraulic-equivalent-diameter-d_458.html
- [20] Capillary number – Wikipedia
https://en.wikipedia.org/wiki/Capillary_number
- [21] Eötvös number- Wikipedia
https://en.wikipedia.org/wiki/E%C3%B6tv%C3%B6s_number
- [22] Weber number – Wikipedia
https://en.wikipedia.org/wiki/Weber_number
- [23] Contact angles – LibreText Chemistry
[https://chem.libretexts.org/Bookshelves/Physical_and_Theoretical_Chemistry_Textbook_Maps/Supplemental_Modules_\(Physical_and_Theoretical_Chemistry\)/Physical_Properties_of_Matter/States_of_Matter/Properties_of_Liquids/Contact_Angles](https://chem.libretexts.org/Bookshelves/Physical_and_Theoretical_Chemistry_Textbook_Maps/Supplemental_Modules_(Physical_and_Theoretical_Chemistry)/Physical_Properties_of_Matter/States_of_Matter/Properties_of_Liquids/Contact_Angles) . On-line (2020)
- [24] How Are Hydrophobicity And Hydrophilicity Measured? – igl coatings
<https://blog.iglcoatings.com/the-science-of-hydrophobicity/> On-line
- [25] Howard H. Hu - Fluid Mechanics (Fifth Edition)
<https://www.sciencedirect.com/topics/materials-science/computational-fluid-dynamics> On-line (2012)
- [26] Computational Fluid Dynamics – Wikipedia
https://en.wikipedia.org/wiki/Computational_fluid_dynamics#Two-phase_flow On-line

- [27] Ignasi Badia Puyol, TFG “Els slats. Estudi d’un element hipersustentador”, UPC, (2019).
- [28] About OpenFOAM – OpenFOAM
<https://www.openfoam.com/> . On-line
- [29] OpenFOAM User Guide – OpenFOAM
<https://www.openfoam.com/documentation/user-guide> On-line
- [30] OpenFOAM Boundary Conditions – OpenFOAM
<https://www.openfoam.com/documentation/guides/latest/doc/openfoam-guide-boundary-conditions.html> On-line
- [31] InterFOAM solver – OpenFOAM wiki
<https://openfoamwiki.net/index.php/InterFoam> On-line
- [32] Carlos Moreno Tavira, “Analysis of two-phase flows under microgravity (spatial) conditions using OpenFOAM”, TFG (2020)
- [33] Capillary Number - Christopher Sparages - OpenWetWare
https://openwetware.org/wiki/Capillary_Number_-_Christopher_Sparages

APPENDIX A. OPENFOAM

In this first appendix the creation of an OpenFOAM simulation will be explained, as well as, how to run it and the ParaView setup used in order to be able to see the results correctly.

A.1 Case folder

In this sub-chapter, the case folder *puntos5* will be shown, which corresponds to velocity $Q_c = 8\mu\text{l}/\text{min}$ and $Q_d = 4\mu\text{l}/\text{min}$. Moreover, it is going to be explained the changes the files experienced depending on the simulation or if they remained the same during the entire project.

A.1.1 0 folder

This is the folder that experienced the most changes, containing the *alpha.oil* (see Fig. A.1), *p_rgh* (see Fig. A.2) and *U* (see Fig. A.3) files, concerning the boundary conditions between the fluids and oil, the pressure and velocity, respectively. All these files start with the heading of OpenFOAM and the dimensions of the parameter chosen. For the dimensions this vector is used [kg, m, s, K, mol, A, cd] and with positive or negative numbers the position is indicated. For example, in the velocity file meters per second (m/s) units are used, so the vector used in the file should be [0, 1, -1, 0, 0, 0, 0].

The meaning of each boundary condition was explained in Chapter 3.1. The boundary conditions for the *alpha.oil* were the most changed in order to find the perfect fit with the contact angles, additionally in the *U* file, the velocity was changed following Table 4.1 and Table 4.2. In order to see all the contact angles used to perform the final simulations from which the data for the plots was taken, check Appendix C.2.2.

```

/*-----*- C++ -*-----
----*\
| ===== |
| \ \ / F i e l d | OpenFOAM: The Open Source CFD Toolbox
| \ \ / O p e r a t i o n | Version: v1806
| \ \ / A n d | Web: www.OpenFOAM.com
| \ \ / M a n i p u l a t i o n |
|-----*\
----*/
FoamFile
{
    version      2.0;
    format       ascii;
    class        volScalarField;
    location     "0";
    object       alpha.oil;
}
// *****
** //

dimensions      [0 0 0 0 0 0 0];

internalField   uniform 1;

boundaryField
{
    inlet1
    {
        type            inletOutlet;
        inletValue      uniform 1;
        value            uniform 1;
    }
    inlet2
    {
        type            inletOutlet;
        inletValue      uniform 0;
        value            uniform 0;
    }
    outlet
    {
        type            zeroGradient;
    }
    wall1
    {
        type            constantAlphaContactAngle;
        theta0          0;
        limit           gradient;
        value            uniform 1;
    }
    wall2
    {
        type            constantAlphaContactAngle;
        theta0          0;
        limit           gradient;
        value            uniform 1;
    }
    wall3
    {
        type            constantAlphaContactAngle;
        theta0          0;
        limit           gradient;
        value            uniform 1;
    }
    wall4
    {
        type            constantAlphaContactAngle;
        theta0          65;
        limit           gradient;
        value            uniform 1;
    }
}

```



```

wall5
{
    type          constantAlphaContactAngle;
    theta0       65;
    limit        gradient;
    value        uniform 1;
}
wall6
{
    type          constantAlphaContactAngle;
    theta0       85;
    limit        gradient;
    value        uniform 1;
}
wall7
{
    type          constantAlphaContactAngle;
    theta0       100;
    limit        gradient;
    value        uniform 1;
}
wall8
{
    type          constantAlphaContactAngle;
    theta0       0;
    limit        gradient;
    value        uniform 1;
}
wall9
{
    type          constantAlphaContactAngle;
    theta0       0;
    limit        gradient;
    value        uniform 1;
}
wall10
{
    type          constantAlphaContactAngle;
    theta0       0;
    limit        gradient;
    value        uniform 1;
}
wall11
{
    type          constantAlphaContactAngle;
    theta0       0;
    limit        gradient;
    value        uniform 1;
}
wall12
{
    type          constantAlphaContactAngle;
    theta0       0;
    limit        gradient;
    value        uniform 1;
}
wall13
{
    type          constantAlphaContactAngle;
    theta0       0;
    limit        gradient;
    value        uniform 1;
}
}

//
*****
//

```

Fig. A.1 *alpha.oil* file


```

wall8
{
    type          fixedFluxPressure;
    value         $internalField;
}

wall9
{
    type          fixedFluxPressure;
    value         $internalField;
}

wall10
{
    type          fixedFluxPressure;
    value         $internalField;
}

wall11
{
    type          fixedFluxPressure;
    value         $internalField;
}

wall12
{
    type          fixedFluxPressure;
    value         $internalField;
}

wall13
{
    type          fixedFluxPressure;
    value         $internalField;
}

outlet
{
    type          fixedValue;
    value         $internalField;
}
}

//
*****
//

```

Fig. A.2 *p_rgh* file

```

/*-----*- C++ -*-----
----*\
=====
  \ \ / / F i e l d           | OpenFOAM: The Open Source CFD Toolbox
  \ \ / / O peration         | Website: https://openfoam.org
  \ \ / / A nd                | Version: 8
  \ \ / / M anipulation      |
\*-----*/
----*/
FoamFile
{
    version      2.0;
    format       ascii;
    class        volVectorField;
    location     "0";
    object       U;
}
// *****
** //

dimensions      [0 1 -1 0 0 0 0];
internalField   uniform (0 0 0);

```

```
boundaryField
{
    inlet1
    {
        type          fixedValue;
        value          uniform (0.0067 0 0);
    }

    inlet2
    {
        type          fixedValue;
        value          uniform (0 -0.0067 0);
    }

    wall1
    {
        type          fixedValue;
        value          $internalField;
    }

    wall2
    {
        type          fixedValue;
        value          $internalField;
    }

    wall3
    {
        type          fixedValue;
        value          $internalField;
    }

    wall4
    {
        type          fixedValue;
        value          $internalField;
    }

    wall5
    {
        type          fixedValue;
        value          $internalField;
    }

    wall6
    {
        type          fixedValue;
        value          $internalField;
    }

    wall7
    {
        type          fixedValue;
        value          $internalField;
    }

    wall8
    {
        type          fixedValue;
        value          $internalField;
    }

    wall9
    {
        type          fixedValue;
        value          $internalField;
    }

    wall10
    {
        type          fixedValue;
        value          $internalField;
    }

    wall11
    {
        type          fixedValue;
        value          $internalField;
    }

    wall12
    {
        type          fixedValue;
    }
}
```

```

        value      $internalField;
    }

    wall113
    {
        type      fixedValue;
        value      $internalField;
    }

    outlet
    {
        type      pressureInletOutletVelocity;
        value      $internalField;
    }
}

//
*****
//

```

Fig. A.3 *U* file

A.1.2 Constant folder

The main files of these folder were changed at the beginning of the project and remained untouched until the end.

One of this files was the *transportProperties* (see Fig. A.4), involving the characteristics of the fluids, where the densities, kinematic viscosities and superficial tension were specified, as decided or calculated in Chapter 2.2. Some others that could also be found in this folder were the *turbulenceProperties* (see Fig. A.5), where the laminar flux was established, and the *g* (see Fig. A.6) one, where the value of gravity was specified to be 0 as mentioned before to ensure microgravity conditions.

This folder also contained another folder (polyMesh) including the characteristics of the specific mesh used, however as it is different for every mesh and geometry, it will not be showed.

```

/*-----* C++ -*-----
----*\
=====
  \ \ / / F i e l d      | OpenFOAM: The Open Source CFD Toolbox
  \ \ / / O p e r a t i o n | Website: https://openfoam.org
  \ \ / / A n d             | Version: 8
  \ \ / / M a n i p u l a t i o n |
\*-----*
----*/
FoamFile
{
    version      2.0;
    format       ascii;
    class        dictionary;
    location     "constant";
    object       transportProperties;
}
// *****
* * //

phases (oil water);

oil
{
    transportModel  Newtonian;
    nu              5.114e-5;
    rho            923;
}

water
{
    transportModel  Newtonian;
    nu              1e-06;
    rho            1000;
}

sigma            0.0301;

//
*****
//

```

Fig. A.4 *transportProperties* file

```

/*-----* C++ -*-----
----*\
=====
  \ \ / / F i e l d      | OpenFOAM: The Open Source CFD Toolbox
  \ \ / / O p e r a t i o n | Website: https://openfoam.org
  \ \ / / A n d             | Version: 8
  \ \ / / M a n i p u l a t i o n |
\*-----*
----*/
FoamFile
{
    version      2.0;
    format       ascii;
    class        dictionary;
    location     "constant";
    object       turbulenceProperties;
}
// *****
* * //

simulationType  laminar;

//
*****
//

```

Fig. A.5 *turbulenceProperties* file

```

/*-----*- C++ -*-----
----*\
=====
  \\\  /  F i e l d           |
  \\\  /  O p e r a t i o n   | OpenFOAM: The Open Source CFD Toolbox
  \\\  /  A n d               | Website: https://openfoam.org
  \\\  /  M a n i p u l a t i o n | Version: 8
/*-----
----*/
FoamFile
{
    version      2.0;
    format       ascii;
    class        uniformDimensionedVectorField;
    location     "constant";
    object       g;
}
// * * * * *
* * //

dimensions      [0 1 -2 0 0 0 0];
value           (0 0 0);

//
*****
//

```

Fig. A.6 *g* file

A.1.3 System folder

This folder includes 5 different files, where four of them remained unchanged during the experiments which are the *decomposeParDict* (see Fig. A.8), the *fvSchemes* (see Fig. A.9), the *fvSolution* (see Fig. A.10) and the *setFieldsDict* (see Fig. A.11). As declared before, in the first one the number of cores is defined, in the second the schemes chosen for the simulations (derivatives, interpolations, etc.), the third one controls the equations solvers, tolerances and algorithms and, lastly, the fourth one sets the fluid's position at the beginning of the experiment.

The remaining file of the system folder, named *controlDict* (see Fig. A.7), experienced some changes, however, the main parts were settled up like Carlos, such as the interval of time the folders were created, or the time format and precision. Other parts such as the simulation time or the time step were changed during the experiments, although to start up it was settled to 0.0512s and to 0.00001s, respectively.

```

/*-----*- C++ -*-----
----*\
===== |
\\      | F i e l d           | OpenFOAM: The Open Source CFD Toolbox
\\      | O p e r a t i o n   | Website: https://openfoam.org
\\      | A n d               | Version: 8
\\      | M a n i p u l a t i o n |
/*-----*-
----*/
FoamFile
{
    version      2.0;
    format       ascii;
    class        dictionary;
    location     "system";
    object       controlDict;
}
// *****
* * //

application    interFoam;

startFrom      startTime;

startTime      0;

stopAt         endTime;

endTime        0.1;

deltaT         0.000005;

writeControl    adjustableRunTime;

writeInterval  0.0004;

purgeWrite     0;

writeFormat    ascii;

writePrecision 6;

writeCompression off;

timeFormat     general;

timePrecision  6;

runTimeModifiable yes;

adjustTimeStep no;

maxCo          2;
maxAlphaCo     1;

}
//
*****
//

```

Fig. A.7 *controlDict* file


```

/*-----*-- C++ -*-----*
-----*\
=====|
\\ \ / | F i e l d | OpenFOAM: The Open Source CFD Toolbox
\\ \ / | O p e r a t i o n | Website: https://openfoam.org
\\ \ / | A n d | Version: 8
\\ \ / | M a n i p u l a t i o n |
\*-----*--
-----*/
FoamFile
{
    version      2.0;
    format        ascii;
    class         dictionary;
    location      "system";
    object        decomposeParDict;
}
// * * * * *
* * //

numberOfSubdomains    6;
method                 scotch;

//
*****
//

```

Fig. A.8 decomposeParDict file

```

/*-----*-- C++ -*-----*
-----*\
=====|
\\ \ / | F i e l d | OpenFOAM: The Open Source CFD Toolbox
\\ \ / | O p e r a t i o n | Website: https://openfoam.org
\\ \ / | A n d | Version: 8
\\ \ / | M a n i p u l a t i o n |
\*-----*--
-----*/
FoamFile
{
    version      2.0;
    format        ascii;
    class         dictionary;
    location      "system";
    object        fvSchemes;
}
// * * * * *
* * //

ddtSchemes
{
    default Euler;
}

gradSchemes
{
    default      Gauss linear;
}

divSchemes
{
    div(rhoPhi,U) Gauss upwind;
    div(phi,alpha) Gauss vanLeer;
    div(phirb,alpha) Gauss linear;
    div(((rho*nuEff)*dev2(T(grad(U)))) Gauss linear;
}

laplacianSchemes
{
    default      Gauss linear corrected;
}

interpolationSchemes
{
    default      linear;
}

```

```

snGradSchemes
{
    default          corrected;
}

fluxRequired
{
    default          no;
    p_rgh;
    pcorr;
    alpha.oil;
}

//
*****
//

```

Fig. A.9 *fvSchemes* file

```

/*-----*-- C++ -*-----*
----*\
=====
  \ \ / / F i e l d           | OpenFOAM: The Open Source CFD Toolbox
  \ \ / / O p e r a t i o n   | Website: https://openfoam.org
  \ \ / / A n d               | Version: 8
  \ \ / / M a n i p u l a t i o n |
-----*--
----*/
FoamFile
{
    version      2.0;
    format       ascii;
    class        dictionary;
    location     "system";
    object       fvSolution;
}
// *****
* * //

solvers
{
    "alpha.oil.*"
    {
        nAlphaCorr      2;
        nAlphaSubCycles 1;
        cAlpha          1;

        MULESCorr yes;
        nLimiterIter    5;

        solver          smoothSolver;
        smoother        symGaussSeidel;
        tolerance       1e-08;
        relTol          0;
    }

    "pcorr.*"
    {
        solver          PCG;
        preconditioner  DIC;
        tolerance       1e-05;
        relTol          0;
    }

    p_rgh
    {
        solver          PCG;
        preconditioner  DIC;
        tolerance       1e-07;
        relTol          0.05;
    }

    p_rghFinal

```


A.2 How to run a simulation

In this subchapter a brief explanation on how the simulations were sent to the EETAC cluster will be done.

- 1- First of all, the case folder had to be sent to the cluster, for that, the following command was used in the personal computers' terminal:

```
scp -r ./OpenFOAM/nuria-8/run/puntos5  
nurialg@147.83.7.212:/cluster/users/students/nurialg
```

- 2- Once in the cluster, it is possible to see the different folders (a) and enter the desired folder (b) using:

```
(a) dir  
(b) cd puntos5
```

- 3- Then the fluids at the initial conditions have to be set, so this command will be used:

```
setFields
```

- 4- Now it is possible to decompose the case to run them in parallel. This will create different folders, depending on the ones decided in the *decomposeParDict* file.

```
decomposePar
```

- 5- After that, everything is ready to start the simulation:

```
mpirun -np 6 interFoam -parallel
```

- 6- When it finishes, the simulation folder has to be reconstructed, so:

```
reconstructPar
```

- 7- As the processors folders do not give any information, they can be deleted. With this command everything starting with *pro* will be deleted, which are just the processor folders.

```
rm -r pro*
```

- 8- The only remaining step is to transfer again the files from the cluster to the personal computer:

```
scp -r nurialg@147.83.7.212:/cluster/users/students/nurialg  
./OpenFOAM/nuria-8/run
```

A.3 ParaView

In this subchapter a brief explanation of the different tools and the setup used for the visualization of the simulations from OpenFOAM, ParaView, will be done.

The first thing that has to be done is opening the .foam file that can be created using this command at the computer's terminal, once the case folder is opened:

```
touch case.foam
```

In order to open ParaView, the only thing that has to be done is using this command at the computer's terminal:

```
paraview
```

After doing that, the simulation at the first time step will be showed. In Fig. A.12 the ParaView window can be seen with the most important parameters that shows.

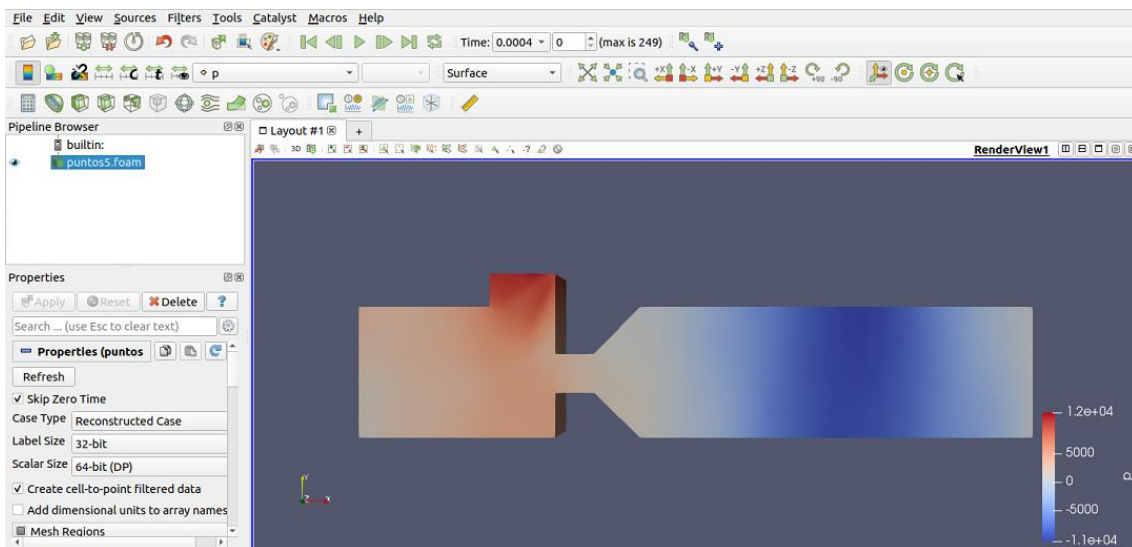


Fig. A.12 General view of the ParaView window

In Fig. A.13 a close-up of the top of the window can be seen. Using the time control part the different folder created with the simulations are displayed and using the buttons it is possible to go to the start or to the end of it, as well as, move forward or backwards one frame. With the display field, the pressure, the velocity or both phases (alpha). For example, in Fig. A.12 the pressure is shown.

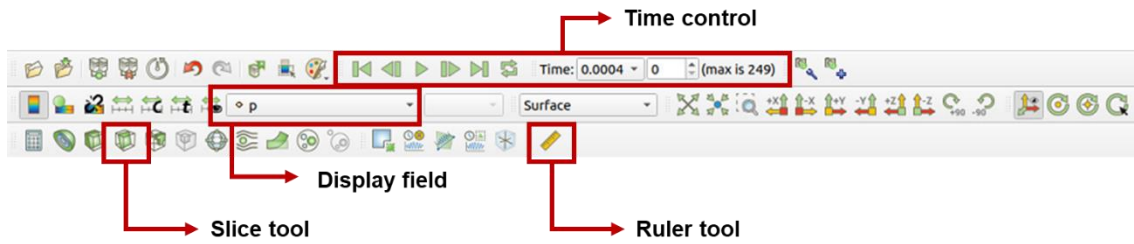


Fig. A.13 Close-up of the top part tools

Now it is important the use of the *slice* tool in order to make a cut in the middle of the geometry and be able to see what is happening inside it (see Fig. A.14). To do that, the slice option has to be chosen and then, the following step is to make a cut in the z-normal direction. Once everything is done the middle section of the geometry can be seen. This step is quite important, because if it is not done, as the water does not stick to the walls, it would not be possible to see the droplets formation.

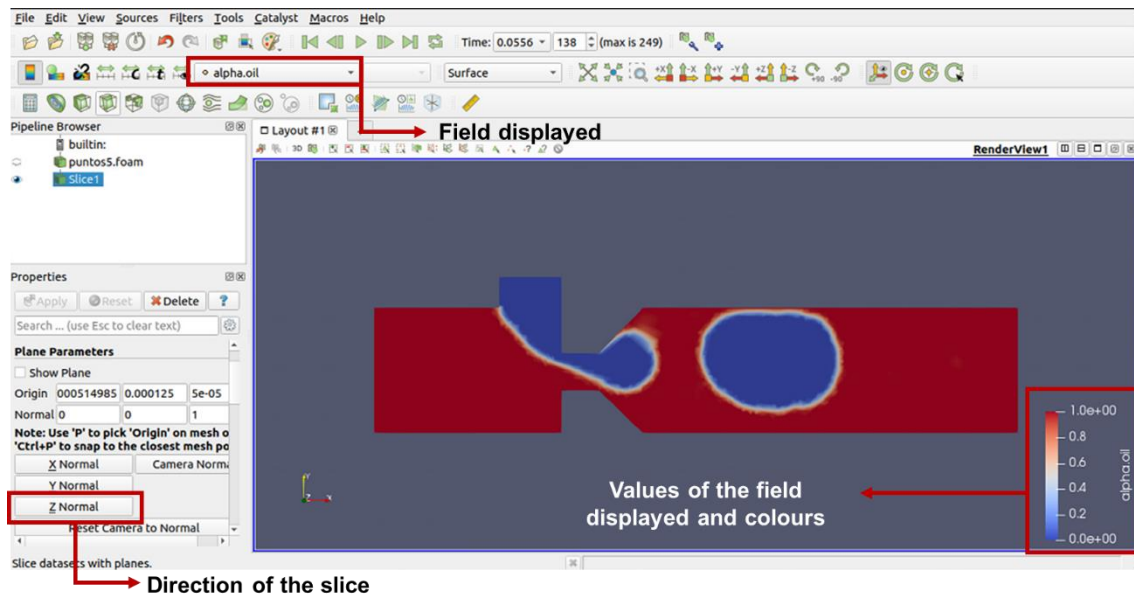


Fig. A.14 ParaView window with the *slice* tool

Another useful and highly used resource this software has is the *ruler* tool which can be seen in Fig. A.15. The measurements of each droplet for the different simulations have been done using this tool. It works in a very simple way, two points are chosen using Ctrl+1, for point 1 and Ctrl+2 for point 2, and ParaView measures the distance from 1 to 2. In Fig. A.15 the horizontal diameter is being measured, however it can also be done with the vertical one and in the same way.

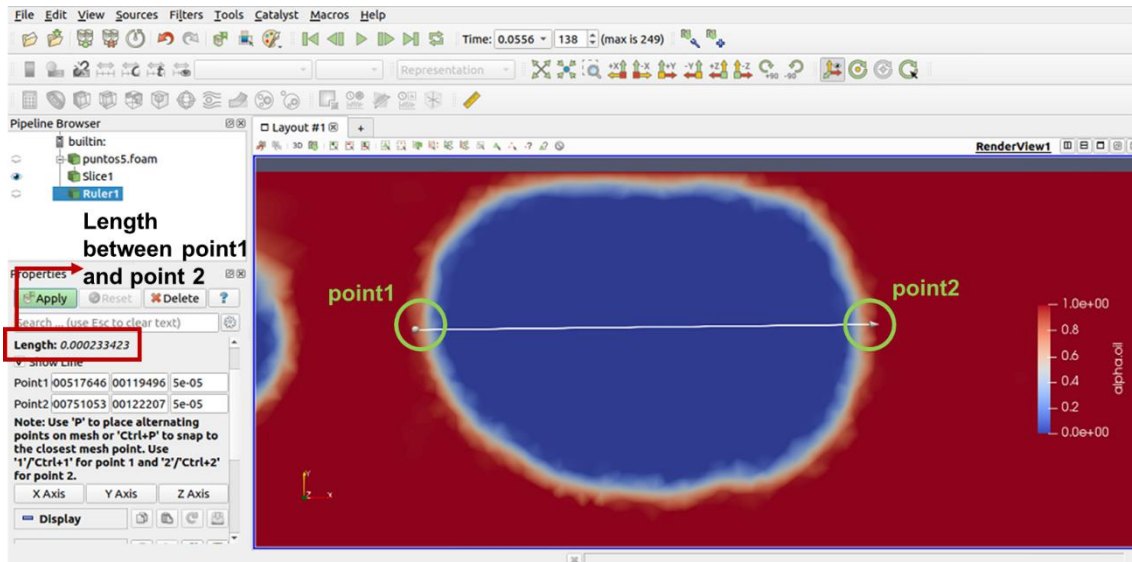


Fig. A.15 ParaView window with the *ruler* tool

APPENDIX B. RESULTS

In this appendix, the tables with all the data gathered from the simulations can be seen. In order to see it more clearly, it has been divided in two tables, Fig. B.2 and Fig. B.3.

Fig. B.1 shows the scheme followed to do the measures. In red, the continuous phase is showed, in white the exaggerated interface of the droplet and in blue the droplet. The sub-index 1 defines the horizontal measures and the sub-index 2 shows the vertical measures.

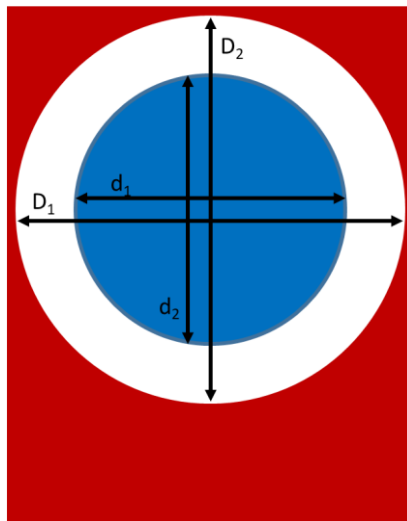


Fig. B.1 Scheme of the droplet for the measures

Here, the symbols used in the following images are going to be clarified:

- $dm1$ and $dm2$: they are simple averages between $d1$ and $D1$ or $d2$ and $D2$ respectively.
- $D12$: is the average between $dm1$ and $dm2$.
- D_{exp} and V_{nexp} : they are the value of the diameter and normalized volume of the experiments, respectively.
- V : is the volume calculated using Eq. 4.1
- V_{nsim} : is the normalized volume, calculated using Eq. 4.2.
- ead and eav : are the absolute error of the diameter and normalized volume, respectively.
- erd and erv : are the relative error of the diameter and normalized volume, respectively.

The first one (Fig. B.2) shows the data extracted directly from ParaView, for this reason it is measured in [m]. It can also be seen that for some specific velocities, there are more than one measure and this is because for that simulation there was more than one droplet formed.

	d1 [m]	D1 [m]	dm1 [m]	d2 [m]	D2 [m]	dm2 [m]	D12 [m]
Qc = Qd = 8 $\mu\text{m}/\text{min}$	0.0002121	0.0002164	0.00021425	0.0002011	0.0001985	0.0001998	0.000207
	0.0001913	0.0001964	0.00019385	0.0001818	0.0001856	0.0001837	0.000189
	0.0001714	0.0001867	0.00017905	0.0001576	0.0001682	0.0001629	0.000171
Qc = Qd = 6 $\mu\text{m}/\text{min}$	0.0002158	0.0002208	0.0002183	0.0002036	0.0002084	0.000206	0.000212
	0.0001965	0.0001999	0.0001982	0.0001872	0.0001934	0.0001903	0.000194
	0.0001813	0.0001962	0.00018875	0.0001674	0.0001729	0.00017015	0.000179
Qc = Qd = 4 $\mu\text{m}/\text{min}$	0.0002059	0.0002083	0.0002071	0.0001948	0.0001979	0.00019635	0.000202
	0.0001885	0.0001931	0.0001908	0.0001778	0.0001815	0.00017965	0.000185
Qc = Qd = 2 $\mu\text{m}/\text{min}$	0.0002019	0.0002041	0.000203	0.0001907	0.0001949	0.0001928	0.000198
	0.0001866	0.0002023	0.00019445	0.0001812	0.0001843	0.00018275	0.000189
Qc = 8 $\mu\text{m}/\text{min}$ Qd = 4 $\mu\text{m}/\text{min}$	0.0001707	0.0001763	0.0001735	0.0001592	0.0001679	0.00016355	0.000169
	0.0001552	0.0001601	0.00015765	0.0001425	0.0001481	0.0001453	0.000151
Qc = 6 $\mu\text{m}/\text{min}$ Qd = 3 $\mu\text{m}/\text{min}$	0.0001804	0.0001862	0.0001833	0.0001753	0.0001799	0.0001776	0.000180
	0.0001634	0.0001686	0.000166	0.0001541	0.0001595	0.0001568	0.000161
Qc = 4 $\mu\text{m}/\text{min}$ Qd = 2 $\mu\text{m}/\text{min}$	0.0001935	0.0001978	0.00019565	0.0001703	0.0001749	0.0001726	0.000184
	0.0001779	0.0001752	0.00017655	0.0001548	0.0001591	0.00015695	0.000167
Qc = 2 $\mu\text{m}/\text{min}$ Qd = 1 $\mu\text{m}/\text{min}$	0.0001859	0.0001807	0.0001833	0.0001625	0.0001609	0.0001617	0.000173

Fig. B.2 First part of the results table

Fig. B.3 shows the continuation of the table shown in Fig. B.2. Here all the measurements are represented in [μm]. The values taken to plot the graphics of Chapter 4 can be seen highlighted in green.

	d1 [μm]	D1 [μm]	dm1 [μm]	d2 [μm]	D2 [μm]	dm2 [μm]	D12 [μm]	Dexp	ead	erd [%]	V [μm^3]	Vn sim	Vn exp	eav	erv [%]
Qc = Qd = 8 $\mu\text{m}/\text{min}$	212.1	216.4	214.25	201.1	198.5	199.8	207.0	158.5	48.5	30.62	2.74E+06	0.69	0.36	0.33	91.86
	191.3	196.4	193.85	181.8	185.6	183.7	188.8	158.5	30.3	19.10	2.24E+06	0.56	0.36	0.20	56.49
	171.4	186.7	179.05	157.6	168.2	162.9	171.0	158.5	12.5	7.87	1.79E+06	0.45	0.36	0.09	25.51
Qc = Qd = 6 $\mu\text{m}/\text{min}$	215.8	220.8	218.3	203.6	208.4	206	212.2	165.5	46.7	28.19	2.90E+06	0.72	0.42	0.30	72.32
	196.5	199.9	198.2	187.2	193.4	190.3	194.3	165.5	28.8	17.37	2.38E+06	0.60	0.42	0.18	41.91
	181.3	196.2	188.75	167.4	172.9	170.15	179.5	165.5	14	8.43	2.00E+06	0.50	0.42	0.08	19.02
Qc = Qd = 4 $\mu\text{m}/\text{min}$	205.9	208.3	207.1	194.8	197.9	196.35	201.7	175.0	26.7	15.27	2.59E+06	0.65	0.45	0.20	43.96
	188.5	193.1	190.8	177.8	181.5	179.65	185.2	175.0	10.2	5.84	2.15E+06	0.54	0.45	0.09	19.19
Qc = Qd = 2 $\mu\text{m}/\text{min}$	201.9	204.1	203	190.7	194.9	192.8	197.9	181.0	22.9	13.09	2.48E+06	0.62	0.53	0.09	17.18
	186.6	202.3	194.45	181.2	184.3	182.75	188.6	181.0	7.6	4.20	2.23E+06	0.56	0.53	0.03	5.34
Qc = 8 $\mu\text{m}/\text{min}$ Qd = 4 $\mu\text{m}/\text{min}$	170.7	176.3	173.5	159.2	167.9	163.55	168.5	144.5	24	16.63	1.74E+06	0.43	0.29	0.15	52.44
	155.2	160.1	157.65	142.5	148.1	145.3	151.5	144.5	6.98	4.83	1.37E+06	0.34	0.29	0.06	19.89
Qc = 6 $\mu\text{m}/\text{min}$ Qd = 3 $\mu\text{m}/\text{min}$	180.4	186.2	183.3	175.3	179.9	177.6	180.5	150.5	30	19.90	2.02E+06	0.51	0.32	0.19	58.16
	163.4	168.6	166	154.1	159.5	156.8	161.4	150.5	10.9	7.24	1.58E+06	0.39	0.32	0.07	23.22
Qc = 4 $\mu\text{m}/\text{min}$ Qd = 2 $\mu\text{m}/\text{min}$	193.5	197.8	195.65	170.3	174.9	172.6	184.1	157.0	27.1	17.28	2.12E+06	0.53	0.36	0.17	47.03
	177.9	175.2	176.55	154.8	159.1	156.95	166.8	157.0	9.75	6.21	1.70E+06	0.42	0.36	0.06	17.85
Qc = 2 $\mu\text{m}/\text{min}$ Qd = 1 $\mu\text{m}/\text{min}$	185.9	180.7	183.3	162.5	160.9	161.7	172.5	166.0	6.5	3.92	1.83E+06	0.46	-	-	-

Fig. B.3 Second part of the results table

APPENDIX C. BOUNDARY CONDITIONS

In this appendix, the boundary conditions used for different stages of the project will be shown.

C.1 Outlet boundary conditions

Fig. C.1 shows the boundary conditions tried for the outlet in Fig. 3.12.

With the name “previous”, the boundary conditions used for the outlet in the previous simulations can be seen. Following that, the rest of the tests performed with these boundary conditions is done. The ones that are written in red are the ones that did not form any droplet. The number between brackets represents the simulation count in Fig. 3.12.

	alpha.oil	p_rgh	U
Previous (1)	zeroGradient	type: fixedValue	type: pressureInletOutlet
		value: \$internalField	value: \$internalField
outlet1 (2)	zeroGradient	type: fixedValue	type: pressureInletOutlet
		value: uniform 0	value: \$internalField
outlet2	zeroGradient	type: fixedValue	zeroGradient
		value: uniform 0	
outlet3	type: fixedValue	type: fixedValue	type: pressureInletOutlet
	value: uniform 1	value: \$internalField	value: \$internalField
outlet4 (3)	zeroGradient	type: fixedValue	type: pressureInletOutlet
		value: uniform 0	value: uniform (0 0 0)
outlet5 (4)	zeroGradient	type: fixedValue	type: inletOutlet
		value: uniform 0	value: \$internalField
		-	inletValue: uniform (0 0 0)
outlet6	zeroGradient	type: fixedValue	type: advective
		value: uniform 0	
outlet7	zeroGradient	type: fixedValue	type: pressureInletOutlet
		value: \$internalField	value: uniform (0 0 0)
outlet8	zeroGradient	type: fixedValue	type: pressureInletOutletParSlipVelocity
		value: \$internalField	value: uniform (0 0 0)
outlet9	zeroGradient	type: fixedValue	type: inletOutlet
		value: \$internalField	value: \$internalField
		-	inletValue: uniform (0 0 0)
outlet10	zeroGradient	type: fixedValue	type: advective
		value: \$internalField	
outlet11	zeroGradient	type: fixedValue	zeroGradient
		value: \$internalField	
outlet12	zeroGradient	type: fixedValue	type: inletOutlet
		value: \$internalField	value: \$internalField
		-	inletValue: uniform (0.005 0 0)

Fig. C.1 Boundary conditions trial

C.2 Contact angles

In this part of the appendix the contact angles for the boundary conditions evaluation and the ones for the results are going to be showed.

C.2.1 Boundary conditions evaluation

Fig. C.2 and Fig. C.3 show all the boundary conditions tried in Chapter 3.2.2.

	walls1	walls2	walls3	walls4	walls5	walls6	walls7	walls8	walls9	walls10	walls11	walls12	walls13
1	85	85	0	105	105	125	125	15	15	15	15	0	0
2	85	85	0	105	105	180	180	15	15	15	15	0	0
3	85	85	0	105	105	175	175	15	15	15	15	0	0
4	85	85	0	105	105	170	170	15	15	15	15	0	0
5	85	85	0	105	105	165	165	15	15	15	15	0	0
6	85	85	0	105	105	160	160	15	15	15	15	0	0
7	85	85	0	105	105	155	155	15	15	15	15	0	0
8	100	100	0	100	100	150	150	15	15	15	15	0	0
9	100	100	0	100	100	145	145	15	15	25	25	0	0
10	100	100	0	100	100	140	140	15	15	35	35	0	0
11	100	100	0	100	100	145	145	15	15	10	10	0	0
12	100	100	0	100	100	145	145	15	15	5	5	0	0
13	100	100	0	100	100	140	140	15	15	10	10	0	0
14	100	100	0	100	100	140	140	15	15	5	5	0	0
15	100	100	0	100	100	135	135	15	15	10	10	0	0
16	100	100	0	100	100	135	135	15	15	5	5	0	0
17	100	100	0	100	100	130	130	15	15	5	5	0	0
18	85	85	0	105	105	140	140	15	15	10	10	0	0
19	85	85	0	105	105	135	135	15	15	10	10	0	0
20	85	85	0	105	105	130	130	15	15	10	10	0	0
21	85	85	0	105	105	125	125	15	15	10	10	0	0
22	85	85	0	105	105	120	120	15	15	10	10	0	0
23	85	85	0	105	105	115	115	15	15	10	10	0	0
24	85	85	0	105	105	110	110	15	15	10	10	0	0
25	85	85	0	105	105	105	105	15	15	10	10	0	0
26	85	85	0	85	85	120	120	15	15	10	10	0	0
27	85	85	0	85	85	115	115	15	15	10	10	0	0
28	85	85	0	85	85	110	110	15	15	10	10	0	0
29	75	75	0	75	75	120	120	15	15	10	10	0	0
30	75	75	0	75	75	115	115	15	15	10	10	0	0
31	75	75	0	75	75	110	110	15	15	10	10	0	0
32													
33	65	65	0	65	65	105	105	15	15	10	10	0	0
34	65	65	0	65	65	100	100	15	15	10	10	0	0
35	65	65	0	65	65	95	95	15	15	10	10	0	0
36	55	55	0	55	55	105	105	15	15	10	10	0	0
37	55	55	0	55	55	100	100	15	15	10	10	0	0
38	55	55	0	55	55	95	95	15	15	10	10	0	0
39	60	60	0	60	60	115	115	15	15	10	10	0	0
40	65	65	0	65	65	115	115	15	15	10	10	0	0
41	60	60	0	60	60	110	110	15	15	10	10	0	0

Fig. C.2 First part of the contact angle trial

42	65	65	0	65	65	110	110	15	15	10	10	0	0
43	90	90	0	90	90	110	110	15	15	10	10	0	0
44	85	85	0	85	85	110	110	15	15	10	10	0	0
45	65	65	0	65	65	65	110	0	0	0	0	0	0
46	65	65	0	65	65	75	110	0	0	0	0	0	0
47	65	65	0	65	65	85	110	0	0	0	0	0	0
48	65	65	0	65	65	95	110	0	0	0	0	0	0
49	55	55	0	55	55	75	110	0	0	0	0	0	0
50	45	45	0	45	45	75	110	0	0	0	0	0	0
51	35	35	0	35	35	75	110	0	0	0	0	0	0
52	25	25	0	25	25	75	110	0	0	0	0	0	0
53	55	55	0	55	55	85	110	0	0	0	0	0	0
54	45	45	0	45	45	85	110	0	0	0	0	0	0
55	35	35	0	35	35	85	110	0	0	0	0	0	0
56	75	75	0	75	75	85	120	0	0	0	0	0	0
57	80	80	0	80	80	90	125	0	0	15	15	0	0
58	85	85	0	85	85	95	130	0	0	20	20	0	0
59	90	90	0	90	90	100	135	0	0	25	25	0	0
60	75	75	0	75	75	95	120	0	0	0	0	0	0
61	80	80	0	80	80	100	125	0	0	0	0	0	0
62	85	85	0	85	85	105	130	0	0	0	0	0	0
63	65	65	0	65	65	100	110	0	0	0	0	0	0
64	65	65	0	65	65	105	110	0	0	0	0	0	0
65	65	65	0	65	65	110	110	0	0	0	0	0	0
66	85	85	0	85	85	130	160	0	0	5	5	0	0
67	105	105	0	105	105	110	150	0	0	0	0	0	0
68	105	105	0	105	105	150	170	0	0	0	0	0	0
69	105	105	0	105	105	110	160	0	0	0	0	0	0
70	85	85	0	85	85	130	130	0	0	0	0	0	0
71	105	105	0	105	105	110	130	0	0	0	0	0	0
72	95	95	0	95	95	110	130	0	0	0	0	0	0
73	105	105	0	105	105	110	120	0	0	0	0	0	0
74	95	95	0	95	95	110	120	0	0	0	0	0	0
75	150	150	0	150	150	110	120	0	0	0	0	0	0
76	130	130	0	130	130	110	120	0	0	0	0	0	0

Fig. C.3 Second part of the boundary conditions trial

Fig. C.4 plots the diameter achieved for each of these simulations, respectively. The x-axis represents the number of simulation and the y-axis the diameter of the droplet generated in that particular simulation. In light green the value of the diameter for each simulation can be appreciated, respectively. For each figure, and shown in red, the experimental value that had to be achieved, which was $166\mu\text{m}$. This plot shows the evolution of the simulations towards the desired goal. There were simulations that performed better solutions than others. However, in general, it can be seen that the changes made on the contact angle improved the measured diameter throughout time, as can be noticed following the tendency line.

It has to be pointed out that there were less than 42 measures, specifically 26, because in some of them the droplet did not break completely, therefore a valid measure of the diameter could not be done.

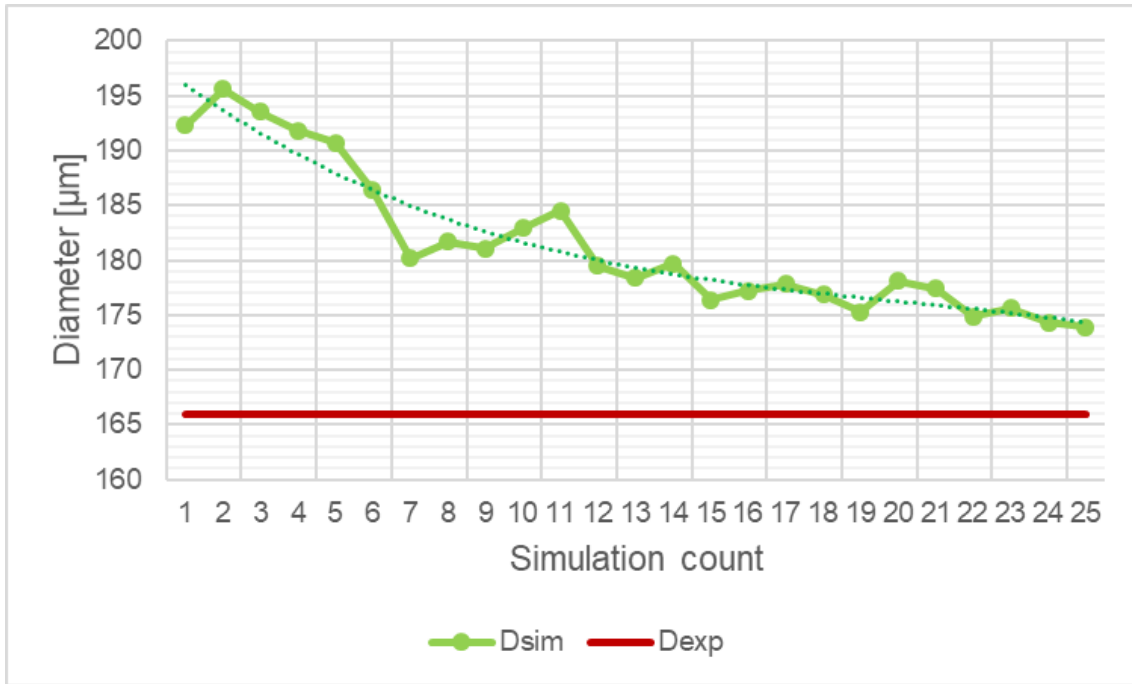


Fig. C.4 Plot of the different normalized volume for every simulation

Fig. C.5 is the continuation of Fig. C.4 where the diameter of the droplet achieved in the simulation was shown. The x-array and the y-array represent the same as before. In this one, 18 more measures were done.

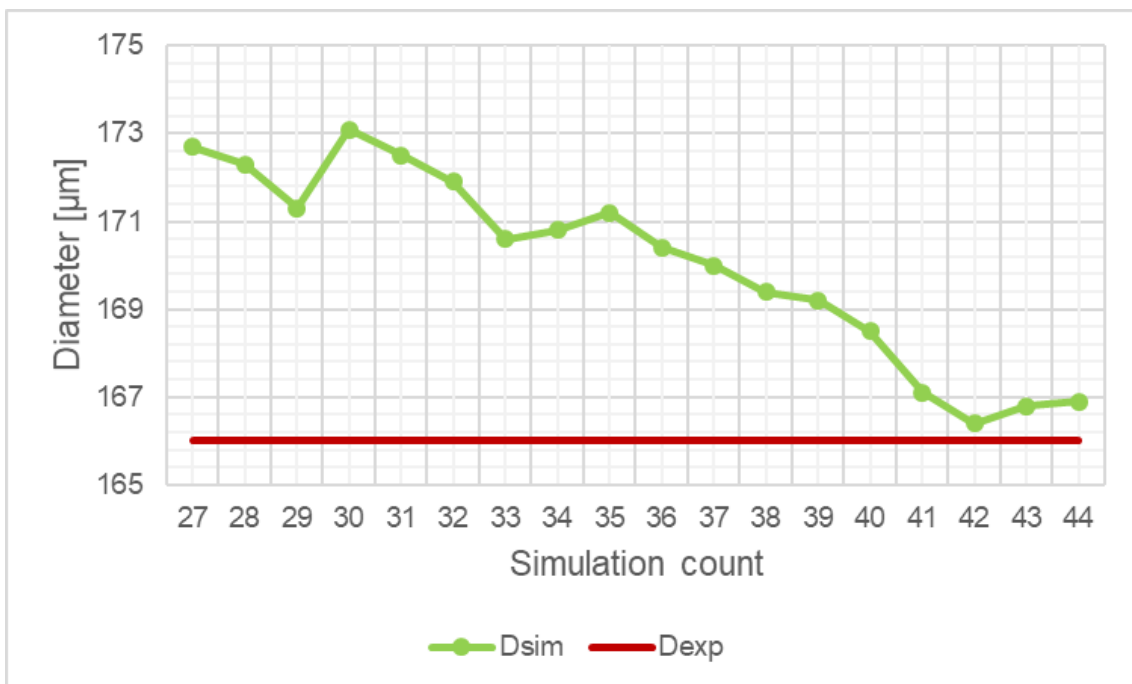


Fig. C.5 Plot of the different diameters for the following simulations

C.2.2 Results

Fig. C.6 shows the contact angles for each wall to achieve the results plotted in Chapter 4.

The first four columns show the results for the same flow rate ratio, $\alpha = 1$. “puntos1” represents velocity $Q_c = Q_d = 8 \mu\text{m}/\text{min}$, “puntos2” represents velocity $Q_c = Q_d = 6 \mu\text{m}/\text{min}$, “puntos3” represents velocity $Q_c = Q_d = 4 \mu\text{m}/\text{min}$ and “puntos4” represents velocity $Q_c = Q_d = 2 \mu\text{m}/\text{min}$. However, the four following columns represent $\alpha = 0.5$. “puntos5” represents velocity $Q_c = 8 \mu\text{m}/\text{min}$ and $Q_d = 4 \mu\text{m}/\text{min}$, “puntos6” represents velocity $Q_c = 6 \mu\text{m}/\text{min}$ and $Q_d = 3 \mu\text{m}/\text{min}$, “puntos7” represents velocity $Q_c = 4 \mu\text{m}/\text{min}$ and $Q_d = 2 \mu\text{m}/\text{min}$ and, finally, “puntos8” represents velocity $Q_c = 2 \mu\text{m}/\text{min}$ and $Q_d = 1 \mu\text{m}/\text{min}$.

	puntos 1	puntos 2	puntos 3	puntos 4	puntos 5	puntos 6	puntos 7	puntos 8
walls1	0	0	0	0	0	0	0	0
walls2	0	0	0	0	0	0	0	0
walls3	0	0	0	0	0	0	0	0
walls4	85	70	55	35	65	45	30	25
walls5	85	70	55	35	65	45	30	25
walls6	65	60	45	35	85	55	40	35
walls7	50	50	40	30	100	70	60	45
walls8	0	0	0	0	0	0	0	0
walls9	0	0	0	0	0	0	0	0
walls10	0	0	0	0	0	0	0	0
walls11	0	0	0	0	0	0	0	0
walls12	0	0	0	0	0	0	0	0
walls13	0	0	0	0	0	0	0	0

Fig. C.6 Contact angles for the final simulations